Trends in Some Characteristics of the Warm-Season Tropopause-Level Jet Streams in Both Hemispheres

Libby J. Orr, Jonathan E. Martin

Department of Atmospheric and Oceanic Sciences, University of Wisconsin–Madison, Madison, WI 53706, USA

Correspondence to: Jonathan E. Martin (jemarti1@wisc.edu)

Abstract. A calendar-year analysis of the isentropic housing of Northern Hemisphere tropopause-level jets is undertaken using three different reanalysis data sets. In contrast to the distinct polar and subtropical jets that characterize the cold season, the analysis reveals that the vast majority of the warm season (May–October) is characterized by a single tropopause-level jet. Additionally, the warm-season jet is found to occupy an isentropic space adjacent to that of the cold-season subtropical jet inviting the interpretation that the traditional polar jet erodes away during the warm-season.

Trends in the waviness, average speed, and latitudinal location of this unimodal warm-season jet are assessed using the recently developed average latitudinal displacement (ALD) methodology. While the results among the various data sets are not as uniform for the warm-season jet as prior work suggests they are for the cold-season polar and subtropical jets, the analysis concludes that the unimodal jet has experienced a slight increase in waviness. Simultaneously, it has undergone a slight decrease in average speed implying that a nearly steady circulation has stirred the NH warm season extratropics over the last 40 years. A similar analysis of the SH warm-season jet reveals that it is also unimodal, has gotten systematically wavier over the same interval and appears to have also sped up on average. Possible implications of these hemispheric differences are discussed.

1. Introduction

Among the most common features of Earth's atmosphere are the tropopause-level wind speed maxima known as jet streams or jets. These narrow streams of fast-moving air represent a fundamental physical and dynamical link between synoptic-scale weather systems and large-scale circulations around the globe. Since the jets play such a substantial role in the production of weather phenomena in the mid-latitudes (e.g., Whitney 1977; Alpert and Ganor 1993; Nakamura and Shimpo 2004; Clark et al. 2009; Athanasiadis et al. 2010; Harnik et al. 2016), they have been the subject of numerous observational studies over time. Both hemisphere's cold seasons (JJAS for the Southern Hemisphere (SH), DJFM for the Northern Hemisphere (NH)), are characterized by the presence of two main jet streams often easily identified at any given time: the subtropical jet and the polar jet. The subtropical jet arises in response to angular momentum transport from the thermally direct Hadley Cell circulation and resides at the poleward edge of the Hadley Cell, at ~30^{o} latitude in the upper troposphere (~200 hPa) (Held & Hou (1980)). The polar jet forms as a result of eddy momentum flux convergence associated with

developing waves within the region of midlatitude baroclinicity (Held 1975; Rhines 1975; McWilliams and Chow 1981; Panetta 1993) and is usually located poleward of ~40° latitude at around 300 hPa (Namias and Clapp 1949; Newton 1954; Palmén and Newton 1969; Keyser and Shapiro 1986; Shapiro and Keyser 1990).

By virtue of their underlying means of formation, the polar and subtropical jets are generally separated both latitudinally and vertically. The jets are also seasonally variable, exhibiting changes in intensity and location (latitudinally) throughout the year. Episodically during the NH extended cold season (November–March), the two jets can become vertically superposed, resulting in a single feature characterized by much faster wind speeds (Christenson et al. 2017, Winters et al. 2020, Handlos and Martin 2021). Another defining characteristic of both species of jets is that they reside near the tropopause, a thermodynamic boundary separating the troposphere from the stratosphere. Observational work by Defant and Taba (1957) found that the NH cold season tropopause has a three-step structure in height from equator to pole with local regions of steep slope occurring at increasingly lower altitudes with increasing latitude. These sharp gradients in tropopause height were also found to be collocated with axes of local wind speed maxima, i.e. the jets.

To characterize the location of the NH tropopause-level jet stream, the present study examines the jet at its location near a "dynamic tropopause" rather than at a pre-ordained height, latitude, or pressure level. Morgan and Nielsen-Gammon (1998) advocated for the use of potential temperature (θ) and wind speed maps on the "dynamic tropopause" [defined as a surface of constant Ertel potential vorticity (PV) (Ertel 1942)] for diagnosing weather systems. When considered from this perspective, the steep tropopause breaks highlighted by Defant and Taba (1957) become regions of large PV gradient on isentropic (θ) surfaces, or large θ gradient on isertelic (constant PV) surfaces, linking them both theoretically (Cunningham and Keyser, 2004; Hoskins et al., 1985) and empirically (Davies and Rossa, 1998; Hoskins and Berrisford, 1988) to the tropopause-level jet cores.

Despite the current broad acceptance of this θ/PV perspective on the tropopause-level jets, there is no clear consensus regarding which isentropic layers serve as characteristic housings for these jet-defining PV gradients. A number of studies (e.g. Defant and Taba 1957, Palmen and Newton 1969, Morgan and Nielsen-Gammon 1998, Shapiro et al. 1999, and Randel et al. 2007), however, suggest a relatively narrow range of likely values for these layers; 335K–345K for the subtropical jet and 310K–320K for the polar jet. More recently, work by Christenson et al. (2017) and Martin (2021) has identified the 315–330K layer for the polar jet and 340–355K for the subtropical jet during the NH extended cold season (NDJFM). Martin and Norton (2023) found the 310–325K layer houses the SH cold season polar jet while the 340–355K layer contains its subtropical jet. Whether or not, and to what degree, these previously identified layers persist as housings for the tropopause-level jets throughout the NH warm season (May-October) and the SH warm season (November – April) is an open question.

A number of prior studies, employing a variety of alternative methods, have considered identification and characterization of trends in the tropopause-level jets. Strong and Davis (2007), through analysis of wind speeds on a "surface of maximum wind", found that Northern Hemisphere jet streams are shifting equatorward while simultaneously increasing in core speed. Archer and Caldeira (2008) utilized mass-weighted average wind speeds in the upper troposphere

to characterize jet streams in both hemispheres. They ultimately reached the conclusion that, in both hemispheres, jet streams have shifted poleward and, in the Northern Hemisphere, weakened in intensity. Manney et al. (2011, 2014, 2017) and Manney and Hegglin (2018) identified jet streams by selecting regions in the upper troposphere in which there is a wind speed maximum greater than 40 m s^{-1}. Jets identified in this manner are bounded wherever the wind speed drops below 30 m s^{-1} and, in the face of multiple areas above 40 m s^{-1} within the selected 30 m s^{-1} regions, jet cores are considered separate only if they are 15° of longitude apart *and* separated by winds less than 25 m s^{-1}. Manney and Hegglin (2018) impose additional latitudinal and thermal characteristics as well, following Manney et al. (2011, 2014). Specifically, they identify the subtropical jet as the most equatorward westerly jet for which the thermal tropopause altitude (using the WMO tropopause definition – see Homeyer et al. (2010)) is both greater than 13 km at the equatorward edge of the jet and drops by at least 2 km across the jet core. The polar jet is then defined as the strongest westerly jet poleward of the subtropical jet, or poleward of 40° latitude if no subtropical jet is identified. Employing these definitions, their analysis found that a relatively steady subtropical jet is moving poleward whereas the polar jet is both weakening and moving equatorward as the planet warms. Though the widely variable methodologies employed in jet identification across studies utilizing reanalysis data have sometimes suggested contradictory conclusions, there is a surprising consensus, among studies employing climate models, that both jets will trend poleward in a warming world (e.g., Barnes & Polvani, 2013; Miller et al., 2006; Swart & Fyfe, 2012; Woollings & Blackburn, 2012; Yin, 2005).

Assessment of jet stream waviness has also been the subject of recent research efforts. Given the physical connection between synoptic-scale weather systems and undulations in the jets, changes in jet stream waviness are likely to lead to changes in daily weather extremes (Röthlisberger et al., 2016). A variety of measures to calculate jet waviness have been developed in recent studies, some utilizing Fourier analyses to assess wave amplitudes (Petoukhov et al., 2013; Coumou et al., 2014; Screen and Simmonds, 2013, 2014) with others focusing on Arctic amplification and its impacts (Blackport & Screen, 2020; Burt et al., 2016; Francis, 2017; Francis et al., 2018; Screen & Simmonds, 2010, 2013; Serreze et al., 2009; Vavrus, 2018). As a result of the wide variety of analysis methodologies, there is little to no consensus on whether a warming world will be characterized by substantial changes in jet structure and waviness (Barnes, 2013; Barnes and Screen, 2015). Recently, Martin (2021) introduced a feature-based metric of waviness, termed the average latitudinal displacement (ALD, to be described later), and applied it to the analysis of the NH and SH (see Martin and Norton, 2023) cold-season tropopause-level jets.

Much of the research devoted to characterizing jet stream behavior in a warming climate has concentrated on the behavior of the cold season jets. Consequently, little work has been devoted to the study of the distribution and characteristics of these features during the warm seasons (May–October in the NH and November–April in the SH). The present research, primarily focused on the NH jets, seeks to investigate aspects of the climatology and long-term trends of the NH warm season tropopause-level jets by first identifying their isentropic location and then applying the ALD waviness metric devised by Martin (2021) to three reanalysis datasets. The paper is organized as follows. A description of the datasets used is given in Section 2. Section 3 presents a theoretical and observational description of the methodology used to

construct the distribution of the tropopause-level jet streams in the NH warm season and examines trends of various characteristics over the past 6 decades. An abbreviated note on results of a companion analysis of the SH warm season jet is also included. A summary and conclusions, along with a discussion of opportunities for future work are presented in Section 4.

2. Data

The ensuing analysis utilizes zonal (u) and meridional (v) winds as well as temperature (T) at 6 h intervals from three different reanalysis data sets: the Japanese 55-year reanalysis (JRA-55), the National Centers for Environmental Prediction/National Center for Atmospheric Research (NCEP/NCAR) reanalysis, and the European Centre for Medium-Range Weather Forecasts (ECMWF) Reanalysis v5 (ERA5). Sixty-one years of data from NCEP/NCAR reanalysis at 17 isobaric levels to 10 hPa on a 2.5° latitude-longitude grid (Kalnay et al. 1996; Kistler et al. 2001) from 1959 to 2019 were used. The JRA-55 data set was employed over the same 61 years (1959-2019) on 60 vertical levels up to 0.1 hPa on a horizontal grid mesh of ~55 km (Kobayashi et al. 2015). Lastly, the ERA5 data on 137 vertical levels from the surface to 80 km with a grid spacing of 31 km covering the 41-year time period of 1979-2019 (Copernicus Climate Change Service [CS3], 2017) was also used. The different reanalyses are the products of varying assimilation schemes and input data sets, with some characterized by known discontinuities arising from the introduction of satellite data (e.g., Santer et al. 1999; Sturaro, 2003). Additionally, the use of data sets with variable start times can complicate the comparison of any resulting time series. The foregoing analysis embraces these differences as evidence of, rather than impediments to, the robustness of the analysis method.

3. Methodology and Analysis Results

3.1 Tropopause-level jets in isentropic space

The first step in the present analysis of the warm season tropopause-level jets is to establish where the jets lie in isentropic space. To make this assessment, the analysis follows aspects of those performed by Koch et al. (2006) and Christenson et al. (2017). First, the maximum wind speed in each grid column of each data set (from 0°N to 80°N) is identified and the corresponding pressure (P_{max}) and potential temperature (θ_{max}) values at the level of maximum wind speed are identified. In constructing their limited climatology, Koch et al. (2006) considered only those grid columns in which the integrated average wind speed between 400 and 100 hPa is greater than 30 m s^{-1}. This same criteria was employed by Christenson et al. (2017), and subsequently by Martin (2021) and Martin and Norton (2023) in their respective work on cold season tropopause-level jet characteristics. Since the jet is usually weaker in the warm season, the number of qualifying columns identified using the 30 m s^{-1} threshold is substantially smaller at that time of year. Therefore, the present analysis

sought a lower threshold for the warm season, the adoption of which would result in a similar number of qualifying columns per month as that characterizing the cold-season analyses previously mentioned. Systematic testing revealed that a warm season threshold of 25 m s^{-1} satisfied this objective. Thus, in the current analysis any column in which the integrated average wind speed exceeds 30 (25) m s^{-1} in the 400–100 hPa layer during NDJFMA (MJJASO)[1] is deemed a *qualifying column*. From such qualifying columns in each data set, θ_{max} is sorted into 5 K bins for the purpose of constructing a histogram of the isentropic distribution of the level of maximum wind for each month of the year. Peaks in the frequency of occurrence in the histograms are then used to determine the characteristic isentropic housings of the jets as in Christenson et al. (2017).

In order to place the analysis results in a proper context, the cold season distribution, originally constructed by Christenson et al. (2017) from the NCEP reanalysis, is also recreated so that a full calendar year climatology of the isentropic distributions of qualifying tropopause-level maximum winds for each month can be examined. Figure 1 displays this full climatology from the JRA-55 data set. A distinct pattern in jet distribution quickly becomes apparent; the warm season is dominated by a single peak in the distribution whereas the cold season has two distinct peaks, representing the polar and subtropical jets, respectively.

The ordinate axes of the histograms measure the fraction of all qualifying columns in each of the prescribed isentropic layers. The warm season exhibits more concentrated peaks, meaning a higher percentage of jet-containing columns fall into these single peaks (Figs. 1e–i). While the cold season features a wider distribution, more than half of all columns are still contained within the two chosen jet layers for all months (Figs. 1a–d, k, and l). Even with the sharper peaks in the warm season, the total percentage of qualifying columns in the chosen 15 K isentropic layer during the warm season is nearly the same as the sum of the discrete polar and subtropical jets' qualifying columns in the cold season. For example, 52% of qualifying columns belong to the polar and subtropical jets in January (Fig. 1a) and 47% of qualifying columns belong to the unimodal jet in August (Fig. 1h).

Christenson et al. (2017) adopted the 315–330 K and 340–355 K layers as the isentropic housings for the cold season polar and subtropical jet, respectively, as these were the peaks in the NCEP reanalysis jet distributions. The isentropic housings of what shall hereafter be referred to as the warm season unimodal jet are selected following the same convention to ensure methodological consistency. These housings fluctuate slightly throughout the course of the warm season. During May, the first month fully characterized by the unimodal jet, 325–340 K is the appropriate layer (Fig. 1e). The jet shifts to the slightly warmer 330–345 K layer for June – September (Figs. 1f-i) but returns to the 325–340 K layer in October. (Fig.1j) to close out the warm season. The percentage of jet-containing columns within the peak of the distribution also fluctuates throughout the course of the warm season. May, characterized by a broader overall distribution, has a peak in which only 37% of all qualifying grid columns reside. This percentage increases to nearly half of all columns (up to 47% in August–Fig. 1h) for the majority of the warm season before falling back to just under 40% in October, the last month with a fully unimodal jet.

[1] For the SH analysis to be presented later, the months defining the cold and warm seasons are inverted.

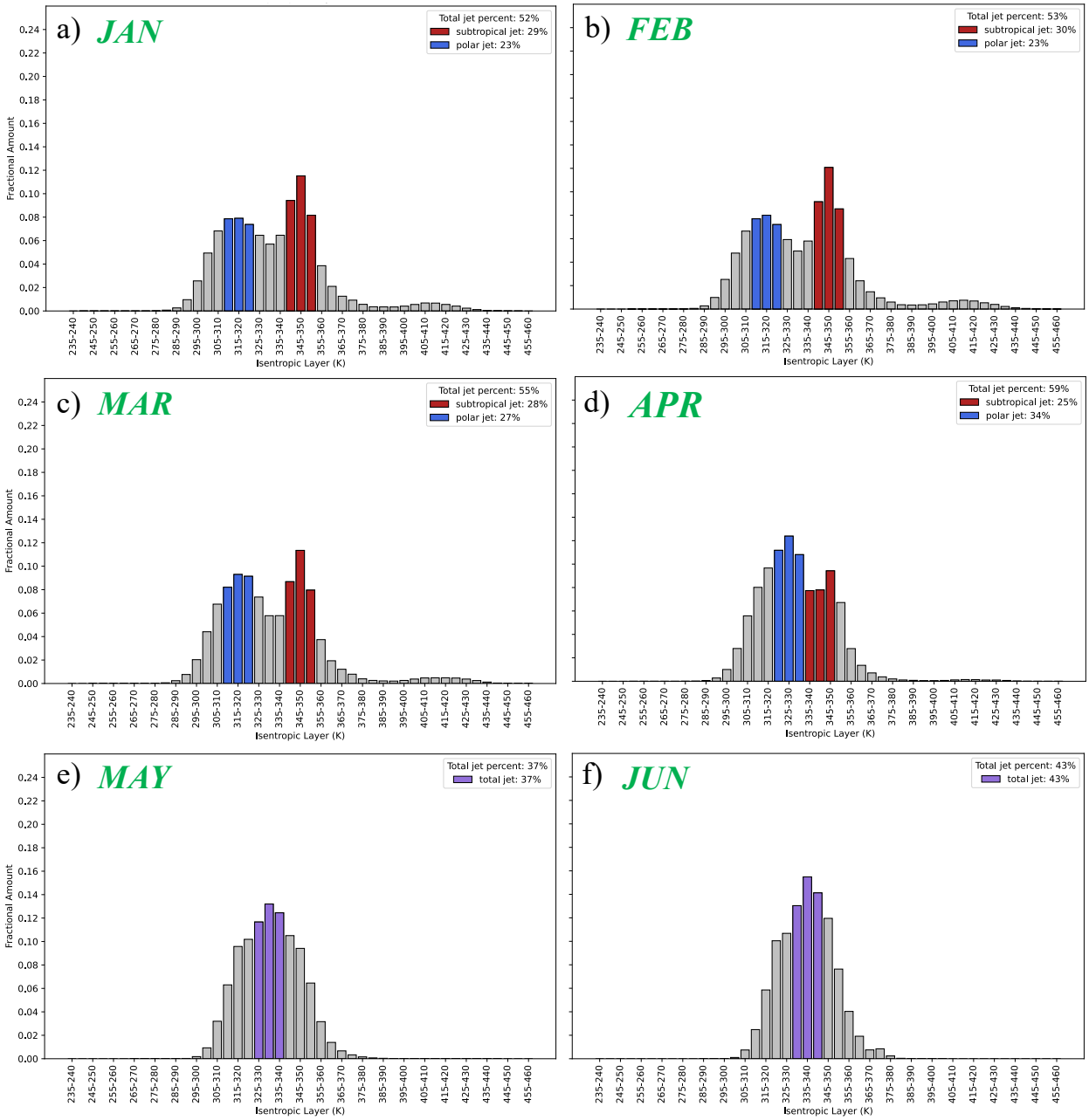

Figure 1: A calendar-year climatology of the Northern Hemisphere tropopause-level jet distribution as depicted by the JRA-55 dataset (see text for explanation). The polar and subtropical jets are represented by blue and red columns, respectively, while the single warm season jet is denoted in purple (Jan. - Jun.).

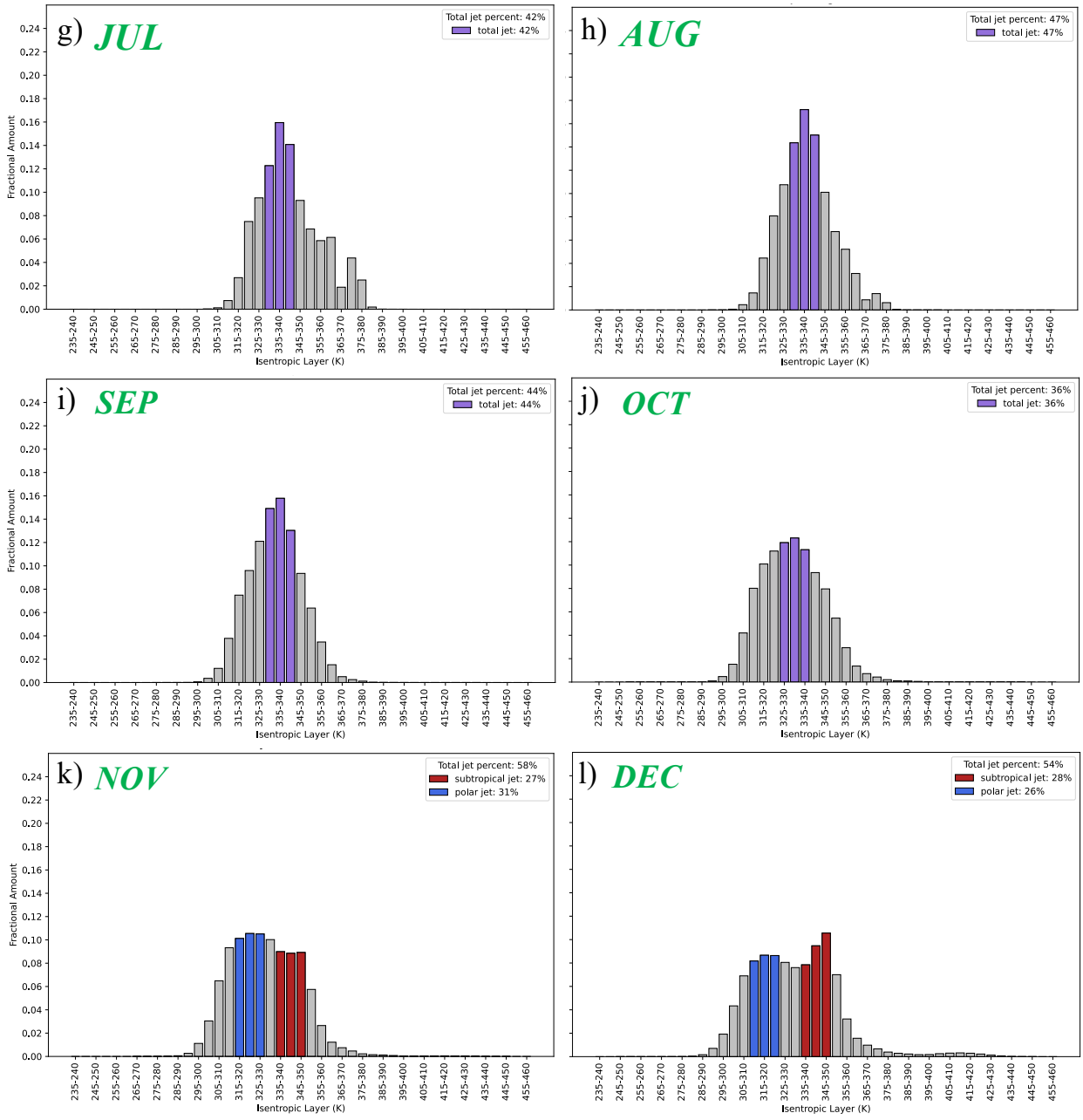

Figure 1 (continued): (Jul. – Dec.)

April and November are transitional months in which the NH jet transforms from a unimodal to bimodal distribution (November) or from a bimodal to unimodal (April). Partitioning April and November into a trio of 10-day average periods sheds more light on the nature of these transitions. Figure 2 illustrates the bimodal to unimodal transition that dominates April. The month starts out as fully bimodal, separate peaks for the polar and subtropical jet separated by a *minimum* in the distribution (Fig. 2a) where a "minimum" is identified if at least one 5 K bin has a lower count of jet-containing columns than those characterizing the adjacent peak(s). The intervening minimum becomes less prominent by April 10th (Fig. 2b) and is completely nonexistent by April 20th (Fig 2c). Finally, by April 30th, any vestige of bimodality is gone and the distribution is distinctly unimodal (Fig. 2d), remaining that way throughout the extended warm season. The opposite transitional pattern unfolds in November, which begins with a broad, unimodal peak (Fig. 3a) at the beginning of the month and develops a distinctly bimodal distribution by November 20 (Fig. 3c) which further matures by the end of the month (Fig. 3d).

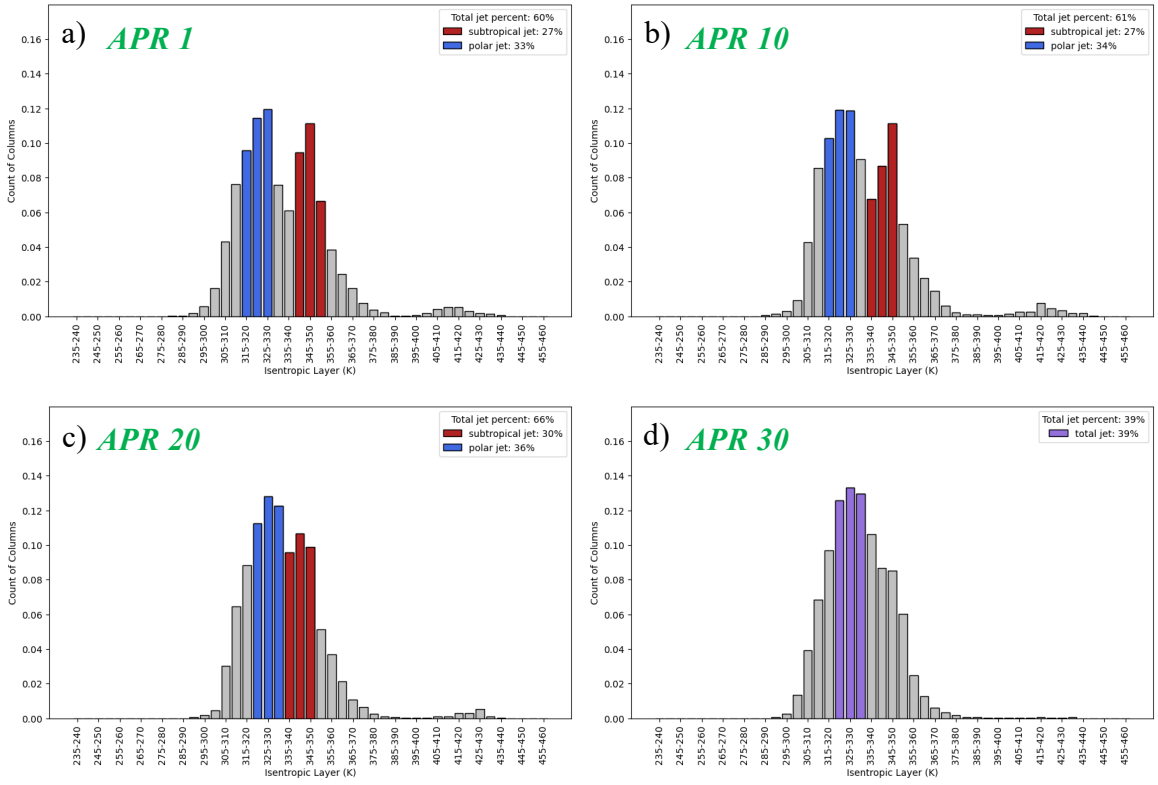

Figure 2: The NCEP Reanalysis portrayal of the tropopause-level jet stream distribution transition from bimodality to unimodality in the month of April, signalling the start of the warm season (May - October). The y-axis is presented at a smaller scale than in prior histogram figures to better depict the modality transition.

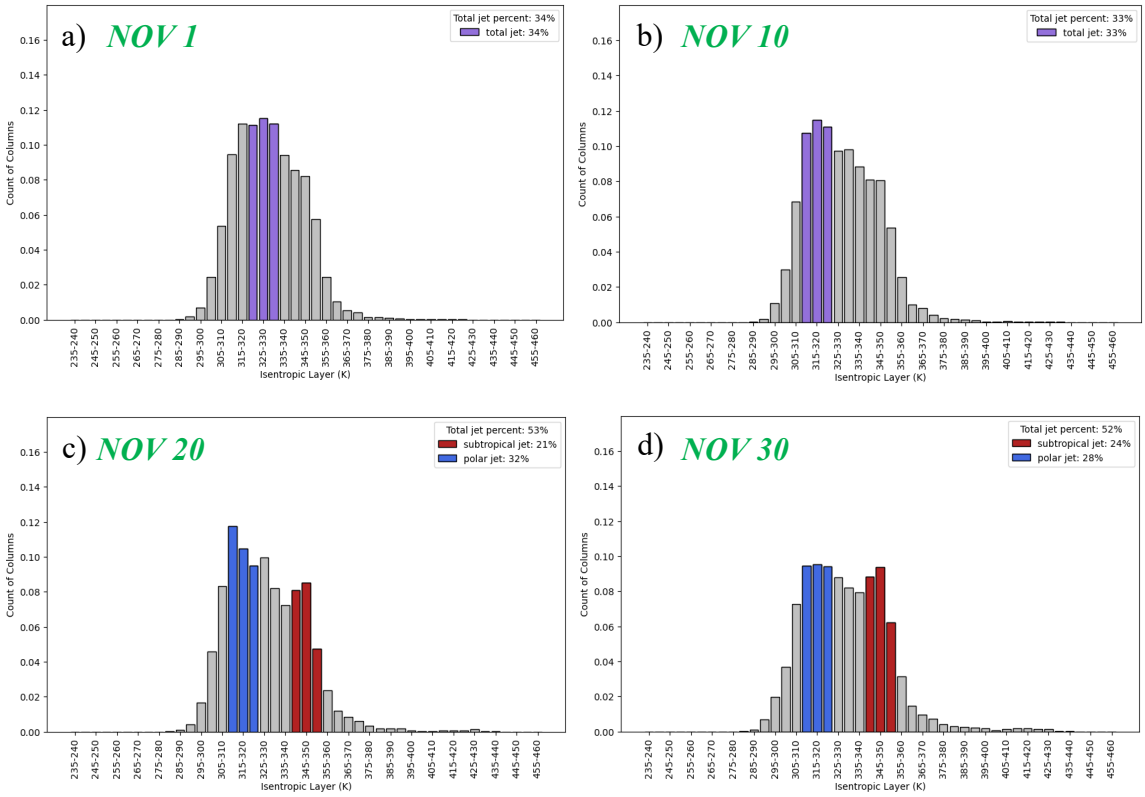

Figure 3: The NCEP Reanalysis portrayal of the tropopause-level jet stream distribution transition from unimodality back to bimodality in the month of November, signaling the start of the cold season (Dec. – Mar.). The y-axis is presented at a smaller scale than in prior histogram figures to better depict the modality transition.

The warm season unimodal jet resides in a rather unique isentropic space between where the cold season polar and subtropical jets are located. Figure 4 compares the jet distribution in January (mid-cold season) to July (mid-warm season) to better exhibit the stark differences between the two. In January, the polar jet occupies the 310–325 K layer whereas the subtropical jet resides at the higher 340–355 K level. The warm season unimodal jet occupies the 330–345 K layer, placing it a slightly lower θ than the cold-season subtropical jet layer. The slight overlap between the warm season unimodal jet layer and the cold season subtropical jet layer invites the interpretation that the polar jet erodes away during the warm season, weakening or disappearing entirely while the subtropical jet persists and, at slightly lower θ, becomes the solitary tropopause-level jet.

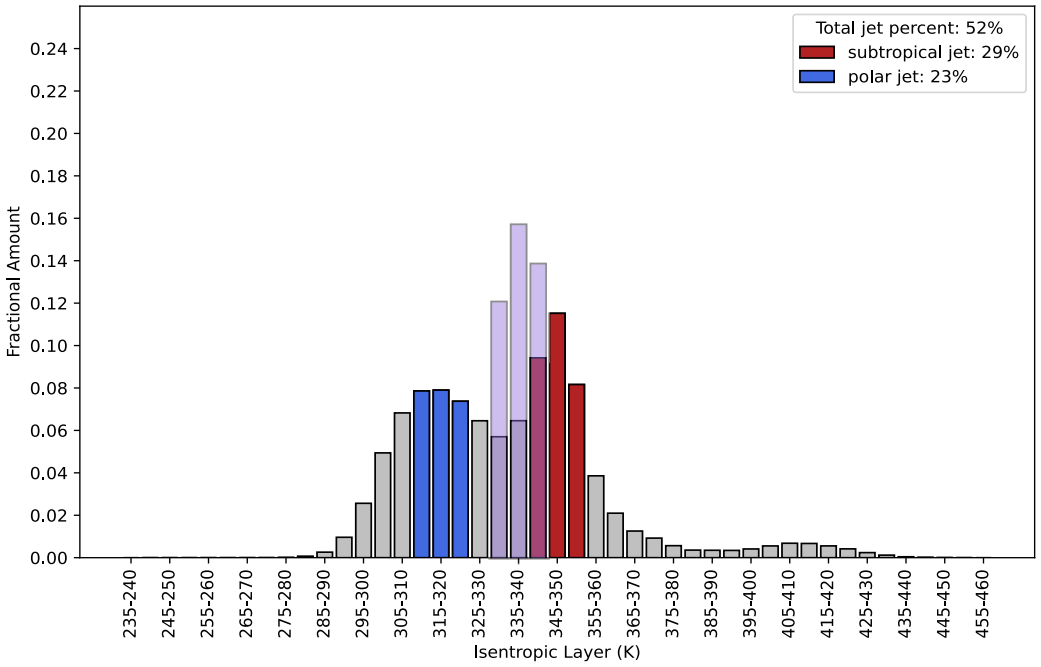

Figure 4: An overlay of the tropopause-level jet distributions for the months of January and July as depicted in the JRA-55 dataset. The peak of the warm season unimodal tropopause-level jet (purple) overlaps a portion of the cold season subtropical jet (red) in isentropic space.

195 The other two data sets (NCEP and ERA5) were subjected to the identical analysis methodology in order to characterize their respective warm season tropopause-level jet distributions. Figures 5 and 6 show the year-long climatology for the ERA5 and NCEP data sets, respectively. Though very particular details of these companion distributions differ slightly, the broad details of the annual cycle of the tropopause-level jet stream(s) are remarkably similar in each of these distinct reanalysis data sets. The three reanalysis data sets exhibit a robust consensus regarding the isentropic location of each jet as
200 illustrated in Table 1, which demonstrates that 91% of all isentropic housings across all three data sets are in agreement.

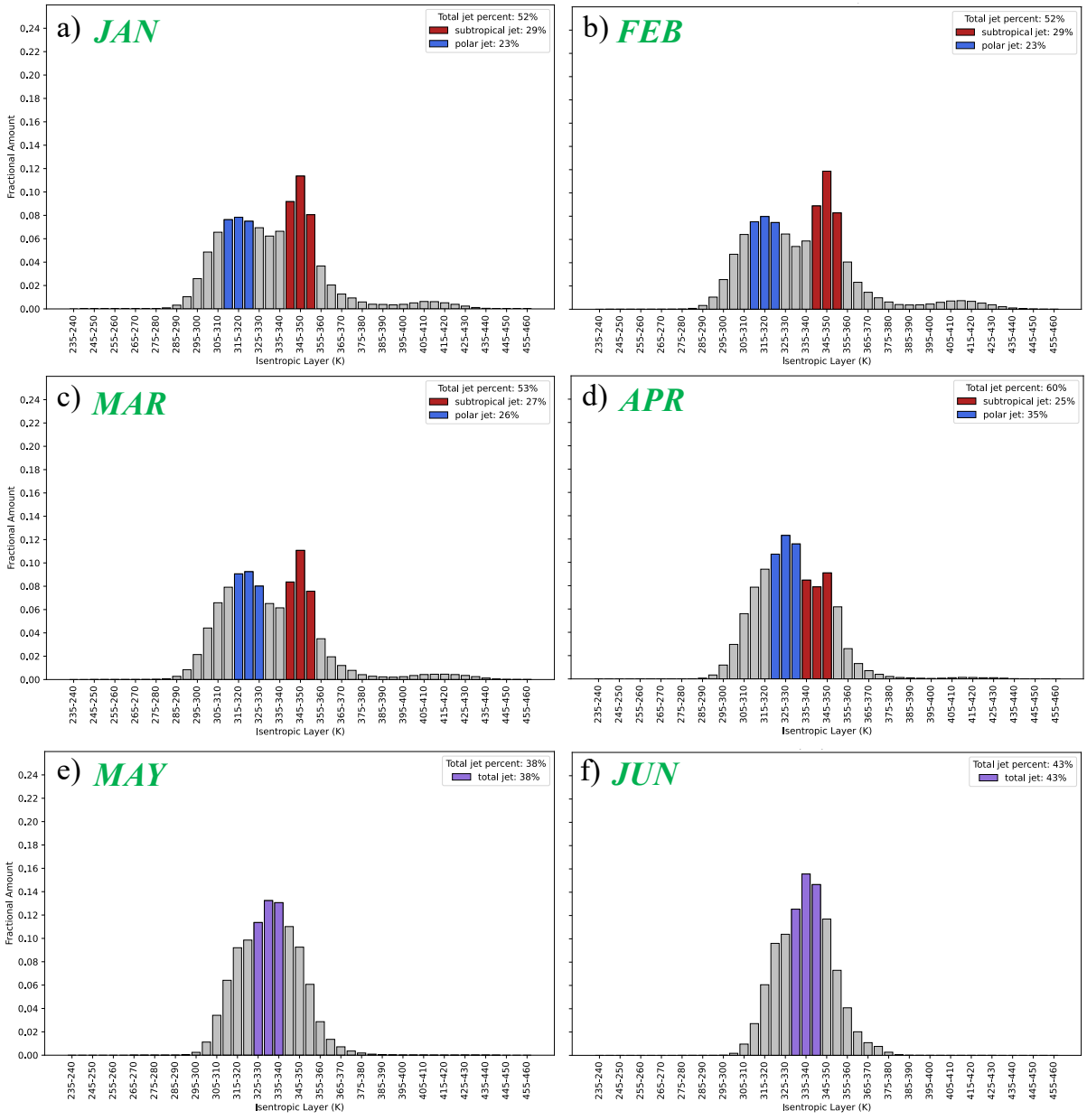

Figure 5: A calendar-year climatology of the Northern Hemisphere tropopause-level jet distribution as depicted by the ERA5 dataset (see text for explanation). The polar and subtropical jets are represented by blue and red columns, respectively, while the single warm season jet is denoted in purple (Jan. - Jun.).

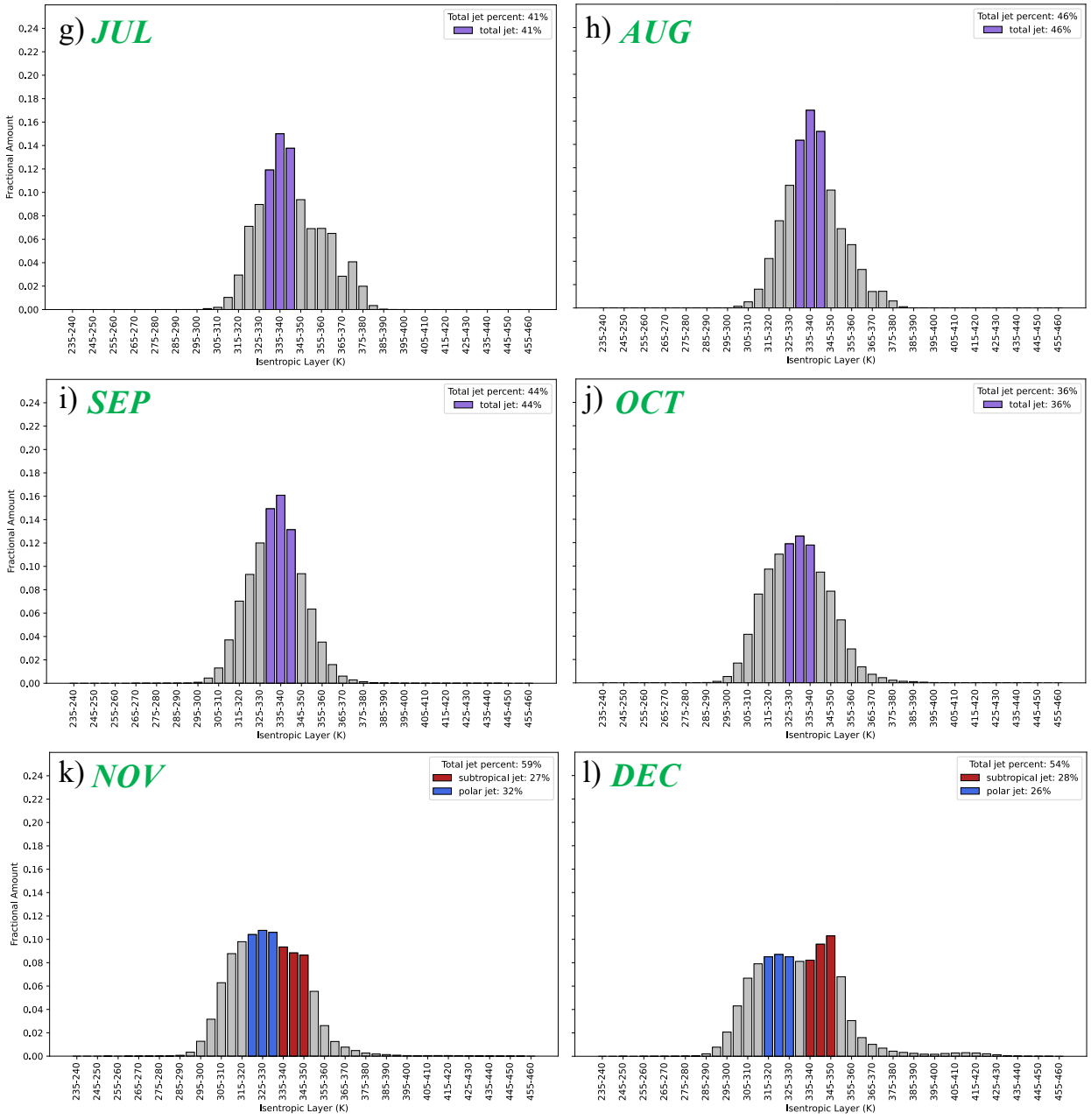

Figure 5 (continued): (Jul. – Dec.)

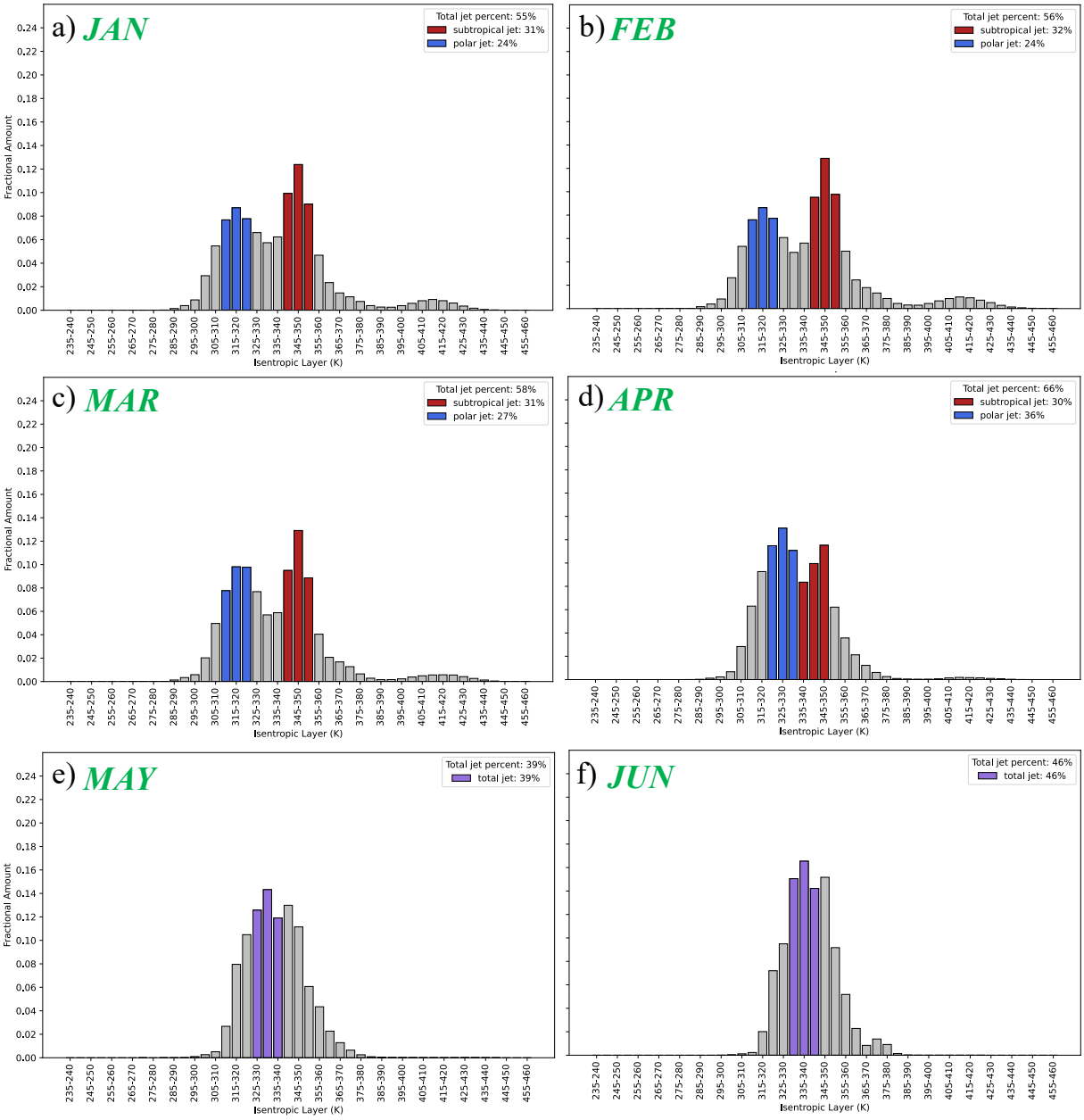

Figure 6: A calendar-year climatology of the Northern Hemisphere tropopause-level jet distribution as depicted by the NCEP dataset (see text for explanation). The polar and subtropical jets are represented by blue and red columns, respectively, while the single warm season jet is denoted in purple (Jan. – Jun.).

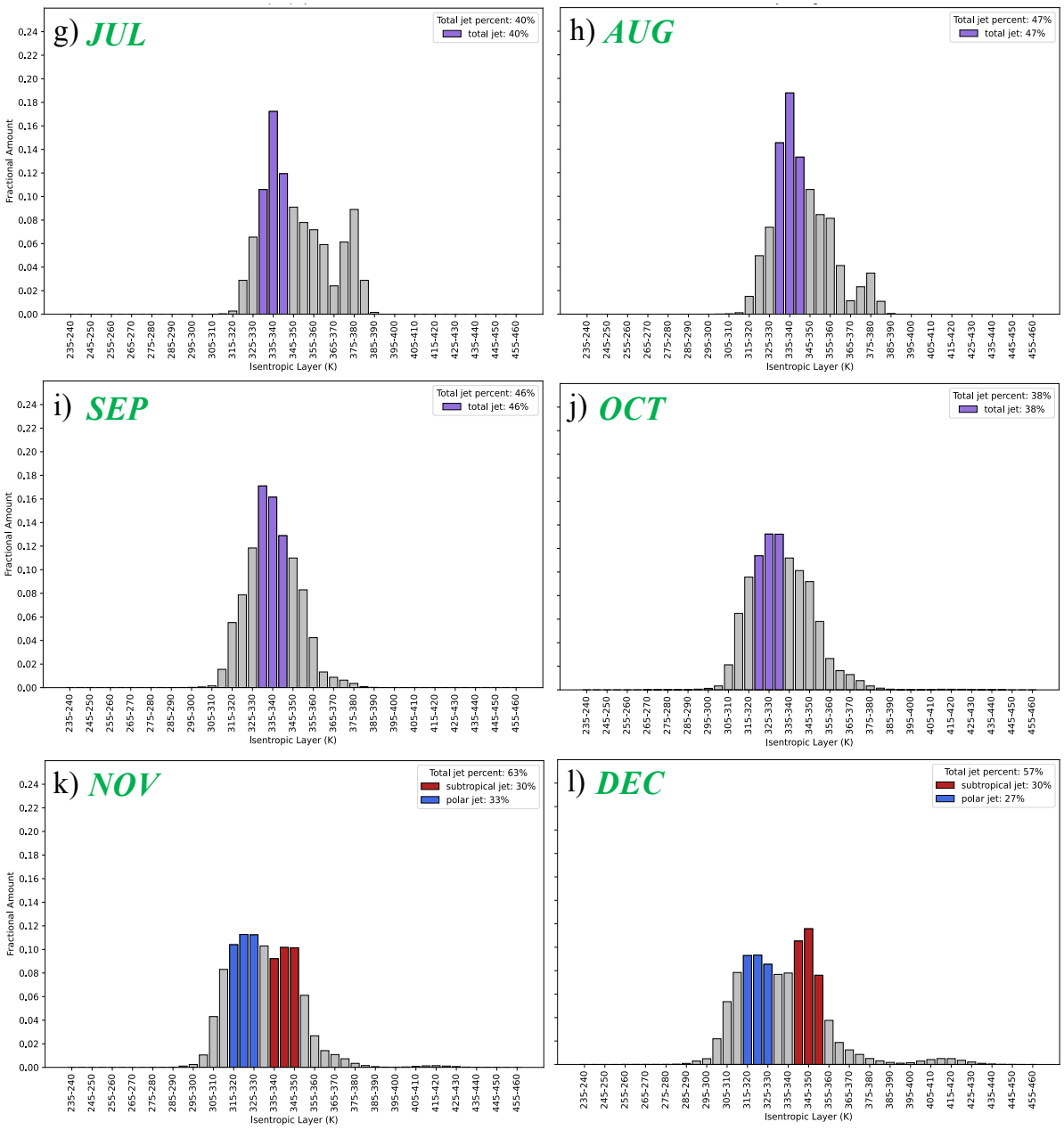

Figure 6 (continued): (Jul. – Dec.)

	NCEP		JRA		ERA	
Month	Polar	Subtropical	Polar	Subtropical	Polar	Subtropical
1	310-325	340-355	310-325	340-355	310-325	340-355
2	310-325	340-355	310-325	340-355	310-325	340-355
3	310-325	340-355	310-325	340-355	**315-330**	340-355
4	320-335	335-350	320-335	335-350	320-335	335-350
5	325-340		325-340		325-340	
6	330-345		330-345		330-345	
7	330-345		330-345		330-345	
8	330-345		330-345		330-345	
9	330-345		330-345		330-345	
10	**320-335**		325-340		325-340	
11	315-330	335-350	315-330	335-350	**320-335**	335-350
12	315-330	**340-355**	**310-325**	335-350	315-330	335-350

Table 1: Isentropic housings of the polar, subtropical, and unimodal jet streams over the course of a calendar year as represented in each of the three reanalysis data sets. Bolded values represent instances in which the isentropic housing in the indicated data set differed from the other two for that species in that month.

Of particular note are the small, but noticeable, peaks at the higher end of the isentropic distribution in July and August for each of the data sets (i.e., Fig. 1g, 1h). These peaks only appeared when lower windspeed thresholds were utilized (i.e. they disappear above the 30 m s^{-1} threshold). Further investigation of these qualifying columns revealed that they generally reside within the same geographical region; a box bounded by roughly 62°E to 95°E and 10°N to 22°N. This region encompasses the Indian subcontinent and surrounding waters. Since the analysis method considers only wind speed, not direction, a likely explanation of these features is that they are associated with the Tropical Easterly Jet (TEJ). The TEJ is characteristic of the upper troposphere (100–150 hPa) within the same geographical area, arises in mid-June, and generally peaks simultaneously with the Indian summer monsoon in July–August (Krishnamurti and Bhalme, 1976; Roja Raman et al. 2009). The notion that these qualifying columns represent the monsoon outflow jet is further supported by the findings of Naidu et al. 2011, in which vertical profiles of zonal winds during both active and weak monsoon seasons depict a peak of easterly jet level winds within this geographical boundary (their Fig. 2).

3.2 Trends in characteristics of the NH warm season unimodal jet

Having identified the isentropic housings of the NH warm season jet, trends in a number of its salient characteristics can be assessed using the average latitudinal displacement (ALD) methodology, devised by Martin (2021). Following Cunningham and Keyser (2004), consideration of the quasi-geostrophic potential vorticity (QGPV) elucidates a direct relationship between PV gradients and strong jet cores. The QGPV is given by

$$q_g = \frac{1}{f_0}\nabla^2\varphi + f + \frac{\partial}{\partial p}\left(\frac{f_0}{\sigma}\frac{\partial \varphi}{\partial p}\right) = \Lambda(\varphi) + f \quad (1)$$

(where $\Lambda = \frac{1}{f_0}\nabla^2 + \frac{\partial}{\partial p}\left(\frac{f_0}{\sigma}\right)\frac{\partial}{\partial p} + \frac{f_0}{\sigma}\frac{\partial^2}{\partial p}$ and φ is the geopotential). Consequently, the cross-jet gradient of QGPV $\left(\frac{\partial q_g}{\partial n}\right)$ can be written as

$$\frac{\partial q_g}{\partial n} = \Lambda\left(\frac{\partial \varphi}{\partial n}\right) = \Lambda\left(-fV_g\right) \quad (2)$$

after substituting in the expression for the geostrophic wind in natural coordinates. This relationship makes clear that large horizontal gradients of tropopause-level PV are collocated with local geostrophic wind speed maxima and is consistent with the observed coincidence of the jet cores with the various "steps" in the tropopause first identified by Defant and Taba (1957).

Given this relationship, it follows that the jet core will reside in a region of strong horizontal PV gradient. Thus, the axis of maximum wind speed of a jet can be approximated by one of several PV contours (isertels) within that strong PV gradient region. The specific isertel will hereafter be referred to as the "core isertel" as it refers to the core of the jet on any given day. To find this core isertel, the circulation, given by

$$C = \oint U \cdot dl \quad (3)$$

is calculated along each isertel ranging from 0.5 to 5 PVU (1 PVU = 10^{-6} m^2 K kg^{-1} s^{-1}) at 0.1 PVU intervals in each jet layer on every day in each data set[2]. Since calculation of the circulation requires measuring contour length, fair comparison among the data sets requires adoption of a uniform horizontal grid spacing. Thus, the horizontal winds from all three data sets were bilinearly interpolated onto isentropic surfaces at 5K intervals (from 300 to 370K) and 2.5º latitude-longitude grid spacing (the lowest native resolution among the three data sets). The daily average PV and average zonal and meridional wind speeds in the unimodal jet layer were then calculated from the 6h data for every day in the three data sets. The isertel along which the circulation per unit length is maximized serves as the core isertel for that given day in that layer. An example of such an objectively identified core isertel in the 330–345 K isentropic layer from the JRA-55 data on May 20, 1995 is illustrated in Fig. 7. Note how the core isertel (with a value of 2.5 PVU) passes directly through the core of the most intense segments of the jet – passing the "eye test".

[2] The isertelic analysis conducted in the companion SH analysis ranges from -0.5 to -5.0 PVU.

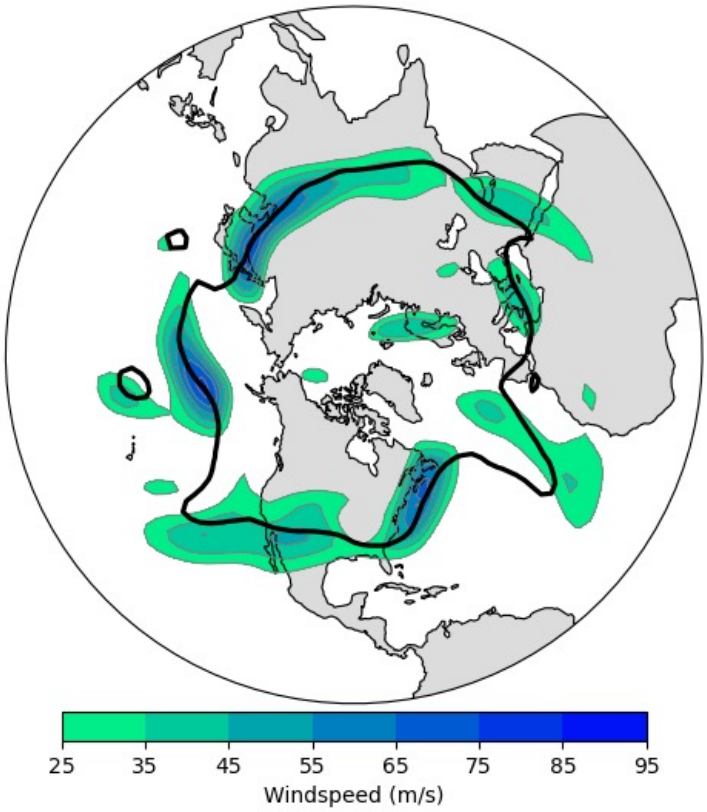

Figure 7: An example of wind speeds (shading) in the 335 – 350 K layer and the corresponding core isertel (black contour) for May 20, 1995, as depicted by the JRA-55 dataset. The physical meaning of, and method for determining, the core isertel are described in the text. For this particular day and layer the core isertel has a value of 2.5 PVU.

Once the core isertel for a jet on a given day in a given layer is determined, the area enclosed within that isertel can be calculated. Next, the latitude of the equatorward edge of a polar cap enclosing an equal area, referred to as the *equivalent latitude*, is calculated as

$$\phi_e = arcsin\left[1 - \frac{A}{2\pi R_e^2}\right] \quad (4)$$

where R_e is the radius of the earth and A is the area enclosed by the core isertel. The meridional displacement of the core isertel from its equivalent latitude at each longitude in the data set can then be measured, as seen in Fig. 8, which revisits the example from May 20, 1995. If an isertel intersects a longitude line multiple times, only segments of the longitude line along which the PV is greater (less) than the core isertel value south (north) of the equivalent latitude are counted. The sum of the length of all these qualifying segments is divided by the number of longitude lines at the resolution of the data (in this case, $2\pi/2.5^o = 144$) and converted to degrees, resulting in what is termed the Average Latitudinal Displacement (ALD).

According to this procedure, a perfectly zonal core isertel (i.e., a zonal jet) would have an ALD of 0.0 with larger numbers representing increasingly wavier jets. Returning to the example case again, the core isertel in Fig. 8 has an ALD value of 5.56°.

Figure 8: Schematic illustrating the meridional displacements of the core isertel from its equivalent latitude from May 20, 1995, using the JRA-55 data set. The equivalent latitude on this day has a value of 34.9° N and is highlighted by the red dashed circular contour. Poleward and equatorward displacements are highlighted as well, in bright red contours and blue contours, respectively.

Consideration of a number of trends in the characteristics of the warm season unimodal tropopause jet proceeds directly from objectively identifying the core isertel for each day in a given season from each data set. It is important to note that the jet's core isertel need not have the same value for each day in a given data set's time series nor across the various data sets on any given analysis day. Consequently, the core isertel distribution in each data set is worthy of additional analysis. Figure 9 displays these distributions for the NH warm season (May–October) jet as seen in all three data sets. Unlike the cold season distributions for the separate polar and subtropical jets in Martin (2021) (see his Fig. 3), there is considerable variability amongst the three data sets in their respective warm season core isertel distributions. The NCEP data set peaks at the lowest PV values, with around 54% of all core isertels in the 61-year period falling within the range of 1.1 to 1.9 PVU. The ERA5 and JRA-55 data sets, in closer agreement with each other, still exhibit substantial differences in their

respective peaks (ERA5 peaks at 2.1 PVU while JRA-55 peaks near 2.5 PVU) though both feature a similarly broader distribution than that seen in NCEP data. Notwithstanding these differences, the peak core isertel values amongst the various data sets exhibit a range of only 1.0 PVU.

We assess the waviness of the warm season unimodal jet using the average latitudinal displacement metric devised by Martin (2021). Figure 10 displays a time series of the seasonal average of daily ALD for each data set calculated over the full NH warm season (May–October). Given that the NCEP and JRA-55 time series are longer than the ERA5, the analysis divided the entire time series into two portions – a pre-satellite era (1958–1979) and a satellite era (1980–2019). Trends from all time series are calculated and the statistical significance of each is evaluated using a two-sided Student's t-test. The interannual variability as well as the overall ALD values are relatively similar across the data sets with NCEP being the largest outlier. Throughout the pre-satellite era both JRA-55 and NCEP suggest a slight reduction in ALD and these trends are significant to at least the 90% level. In the satellite era, all three reanalyses suggest an increase in waviness though only the slightly steeper NCEP and ERA-5 times series are significant. And, though the NCEP ALD is systematically ~1.0º greater than its corresponding ERA-5 counterpart, the increase in waviness to which both time series attest is quite modest, on the order of ~0.3º over ~40 years. Though the JRA-55 trend is not significant, it is similarly modest. Overall, we conclude that the warm season unimodal tropopause jet has undergone a very slight increase in waviness over the past 4 decades.

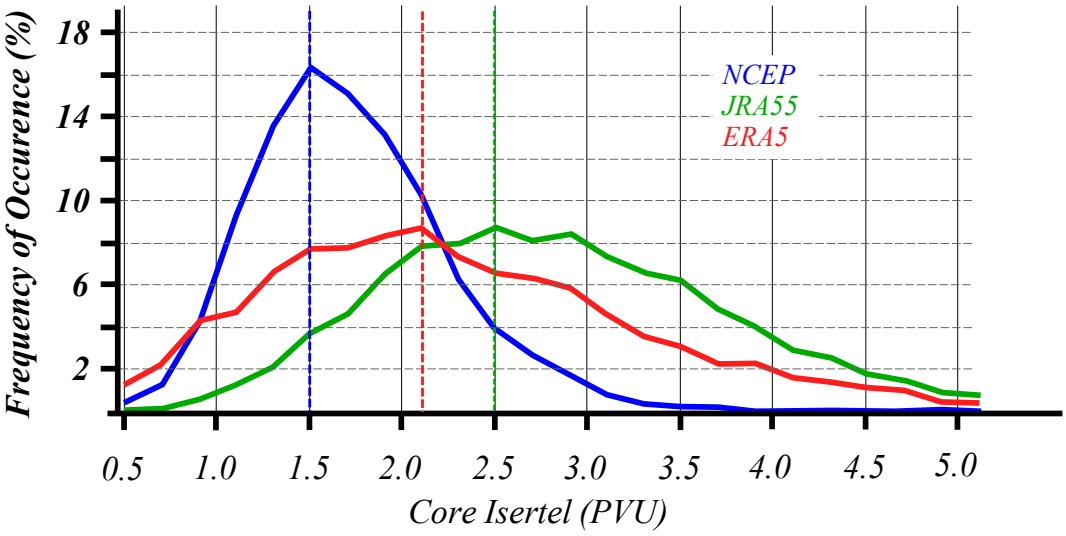

Figure 9: Frequency of occurrence of core isertel value for each reanalysis dataset during the Northern Hemisphere warm season (May - October). Isertel values given in potential vorticity units (PVU, 1 PVU = 10^{-6} K m^2 kg^{-1} s^{-1}).

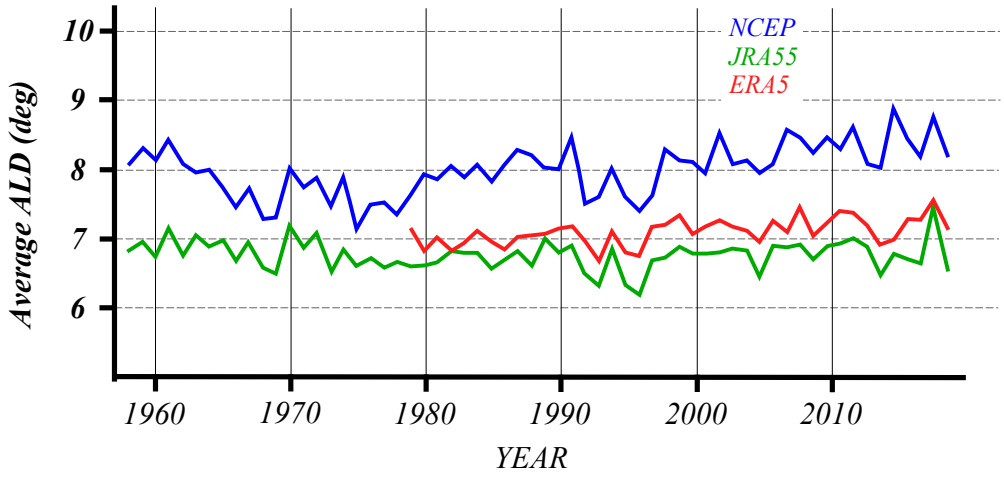

Figure 10: Seasonal average ALD (in degrees) of the Northern Hemisphere unimodal warm season jet (May - October) for each of the different reanalyses.

As mentioned in describing the ALD method, the core isertel is defined as the isertel along which circulation per unit length is maximized, delegating it as the core of the jet. Consequently, it is safe to assert that the average wind speed along a given day's core isertel represents the average jet speed on that day[3]. The time series of seasonal average (May–October) speed for each data set is portrayed in Fig. 11. Once again, the overall time series appears to have two distinct portions – pre-satellite and satellite eras. The average wind speed increases slightly in the pre-satellite era as documented by the NCEP and JRA-55 data sets. These increases are statistically significant to the 95% level. The slight decrease in the satellite era, represented in all three data sets, is statistically significant only in the ERA5 data set. Overall, given the mixed verdict regarding significance and the meager magnitude of the changes in both portions of the total time series, it appears that the average speed of the warm season unimodal jet has hardly changed over the documented interval.

Identification of the core isertel leads directly to the calculation of daily values of equivalent latitude, which is very nearly the zonally averaged latitude of the jet core on any given day. The time series of the seasonal average equivalent latitude (May–October) for the NH unimodal jet for each data set is shown in Fig. 12. The NCEP time series consistently portrays a more poleward warm season jet core than that JRA-55 or ERA5. The latter two reanalyses, however, depict very similar time series of the equivalent latitude of the warm season jet core. Though the slight equatorward migration of the jet

[3] Though only grid columns with a 100–400 hPa integrated average wind speed exceeding 25 m s^{-1} are counted in construction of the defining histogram, the core isertel spans the entire hemisphere and so includes regions where the wind speed is less than 25 m s^{-1}.

core in the pre-satellite era is statistically significant, the nearly flat trend characterizing the satellite era is not significant in any of the three reanalysis data sets. Thus, the analysis suggests that the core of the warm season unimodal tropopause-level jet has simply alternated between 40° and 42° latitude over the past 4 decades.

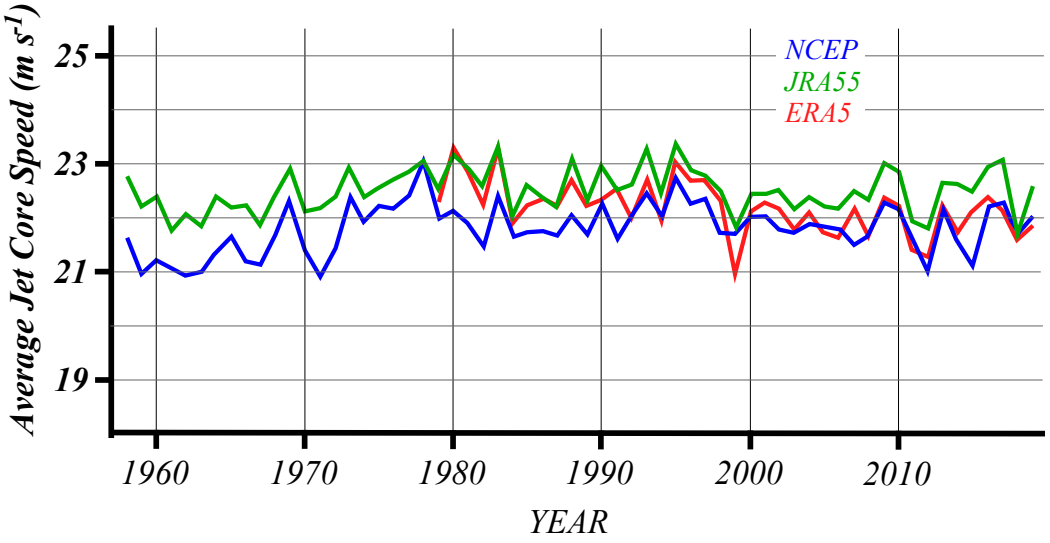

Figure 11: Average wind speed (m s^{-1}) along the core isertel of the Northern Hemisphere warm season (May - October) unimodal jet for each of the different reanalyses.

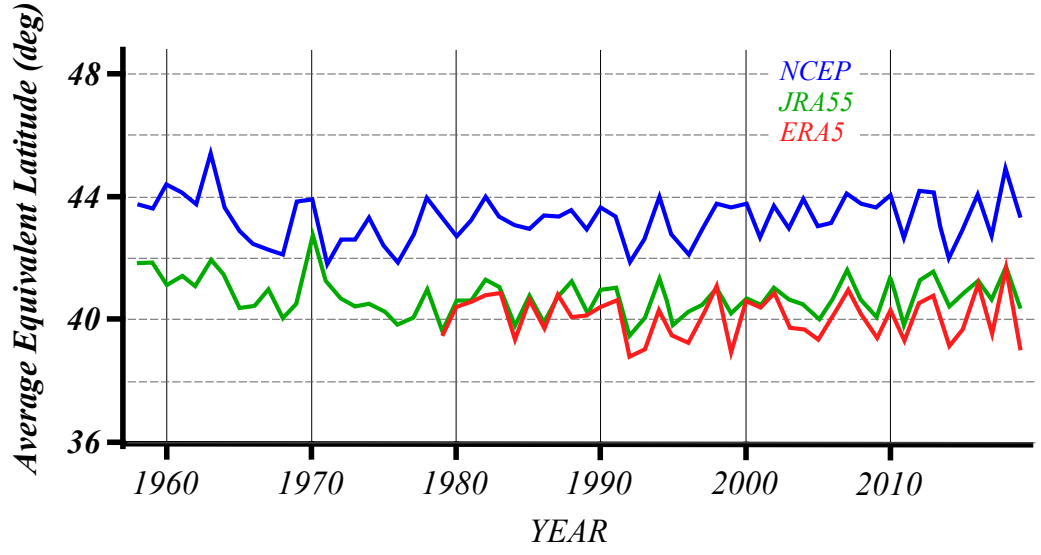

Figure 12: Seasonal average equivalent latitude of the Northern Hemisphere unimodal warm season (May - October) jet for each of the different reanalyses.

3.3 A note on characteristics of the SH warm season jet

Employing the method previously described, Martin and Norton (2023) considered the climatology of the cold season Southern Hemisphere tropopause-level jets. Here we interrogate the isentropic distribution of the warm season SH jet and several of its characteristics. In the interests of brevity, only the monthly JRA55 histograms of SH jet distributions are shown in Fig. 13. The annual cycle of SH tropopause-level jets is seen to mirror that of the NH with a clear bimodality throughout the extended cold season (MJJAS) and a unimodal jet throughout the extended warm season (NDJFM). The transition periods in the SH occupy late April/early May and most of October (not shown). In addition, extending the isentropic analysis to higher θ values, the polar night jet appears weakly as a third peak in the histogram in May, strongly in JASO, and then gradually weakens to nothing by December. Though not shown, the other two data sets are nearly identical in their depiction of this annual cycle with only slight variations in the isentropic housings of the jet(s) during a few months – as was shown to be the case for the NH distribution.

The analysis reveals that the NDJFM unimodal SH jet is as wavy as its NH counterpart, with all three data sets exhibiting a significantly upward trend in waviness (Fig. 14). Thus, it appears that the SH warm season tropopause-level jet has gotten systematically wavier over the past 4 decades. Analysis of the average jet core wind speed suggests that the SH warm season jet is not only faster than its NH counterpart but also exhibits substantially less interannual variability (Fig. 15). Despite the fact that all 3 data sets display a positive trend, the rates are quite different and only the JRA55 and NCEP trends are statistically significant. Consequently, though the signal is somewhat mixed, the analysis suggests that the SH warm season unimodal jet is speeding up.

Finally, Fig. 16 depicts a slight poleward trend in the equivalent latitude of the SH warm season unimodal jet, especially in the satellite era, though only the JRA-55 trend is statistically significant. Thus, quite like the NH warm season jet, the SH unimodal jet has been rather stationary (at 47°S) for the last 4 decades. It is notable, however, that the SH feature exhibits considerably more interannual variability than its NH counterpart.

The striking differences in variability in both average jet core speed and equivalent latitude between the NH and SH warm season jets are of considerable interest. With regard to the jet core speed differences, it may be that the SH warm season jet exhibits, on average, a more continuous ribbon of high wind speed around the hemisphere — that is, a more uniform jet envelope — than its NH counterpart. If true, such uniformity might account for the higher annual average wind speed. Were there, however, substantial variability in the uniformity of the jet envelope, then the average jet core speed would likely reflect that variability.

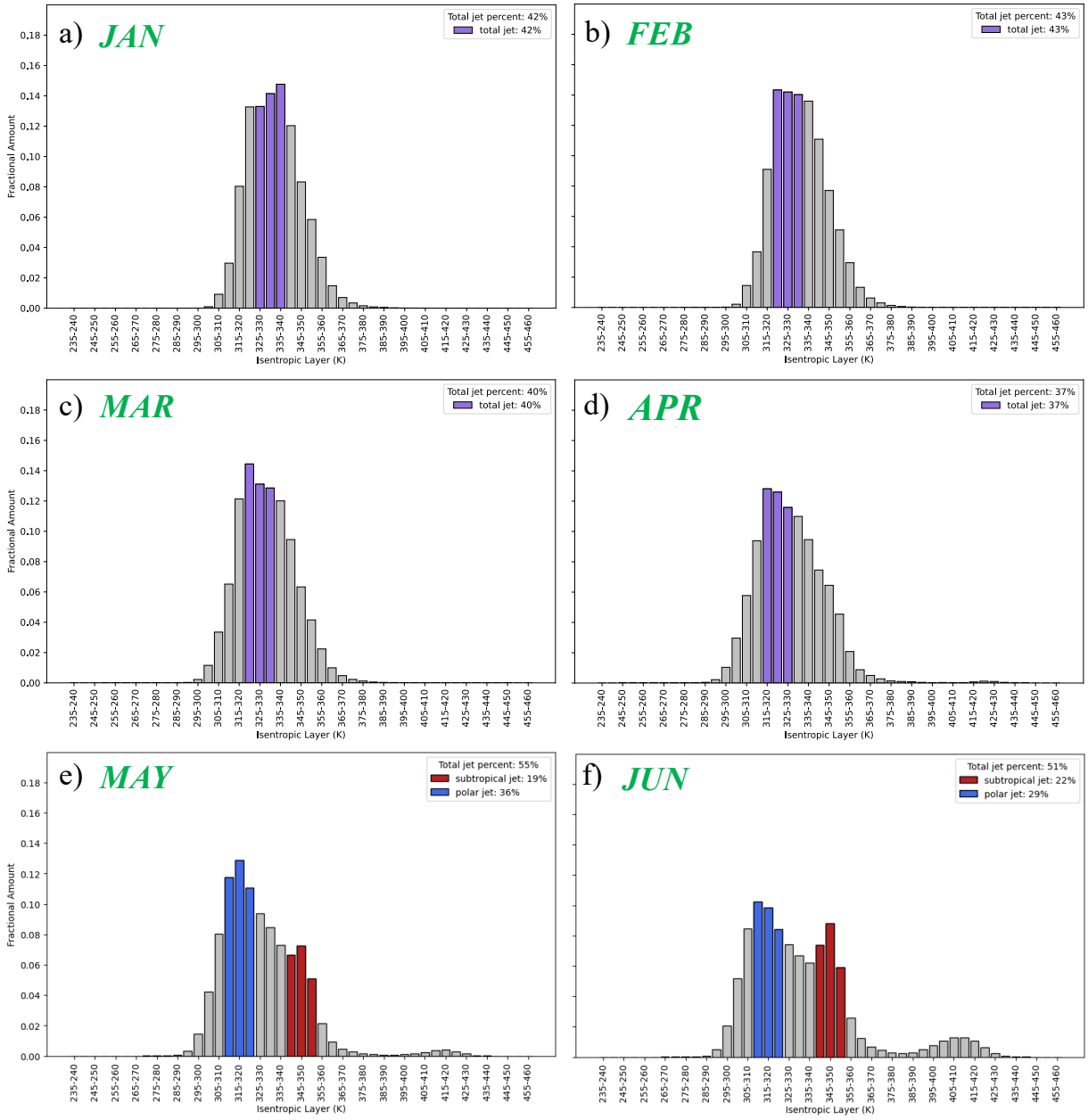

Figure 13: A calendar-year climatology of the Southern Hemisphere tropopause-level jet distribution as depicted by the JRA-55 dataset (see text for explanation). The polar and subtropical jets are represented by blue and red columns, respectively, while the single warm season jet is denoted in purple.

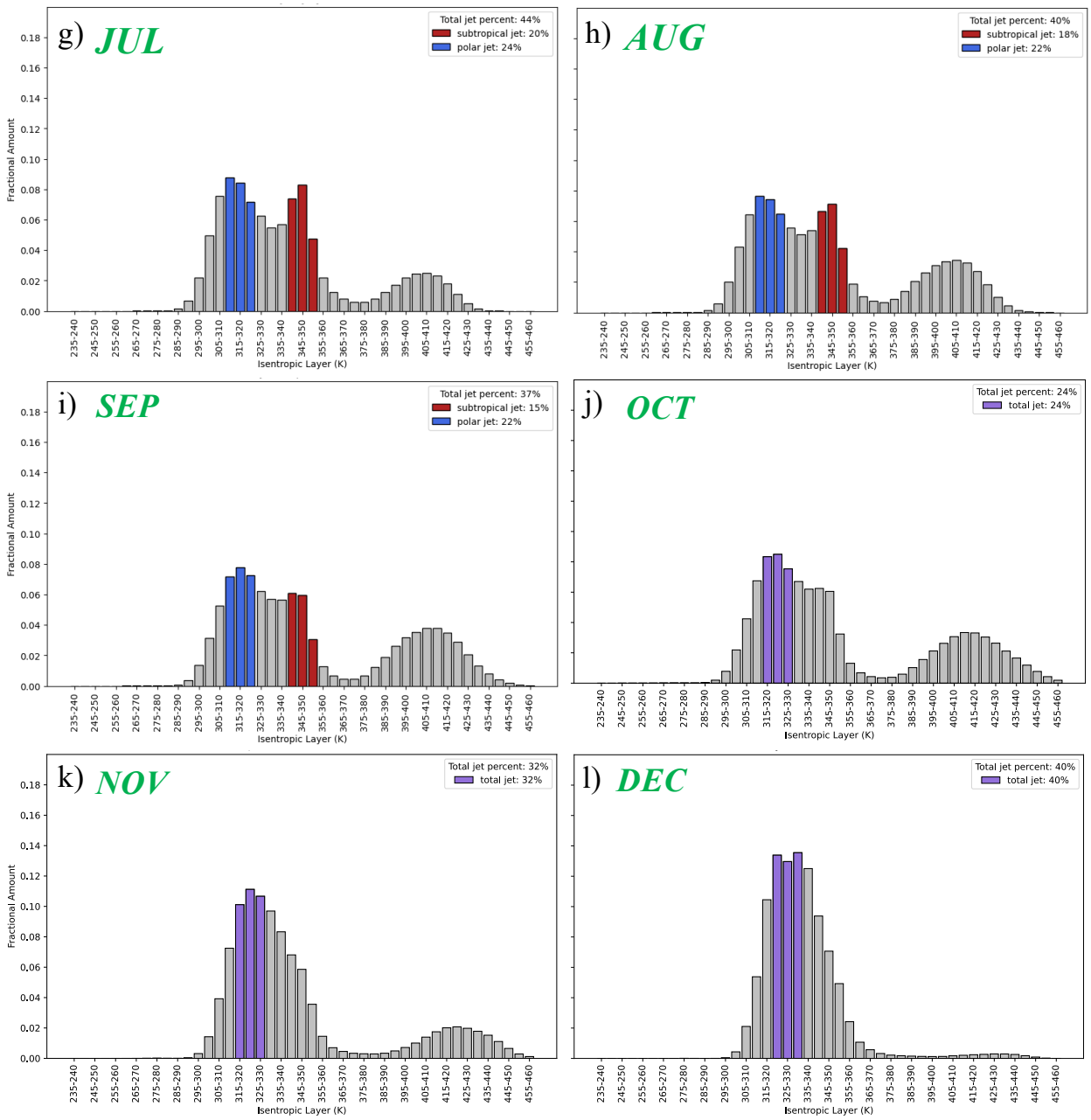

Figure 13 (continued): (Jul. – Dec.)

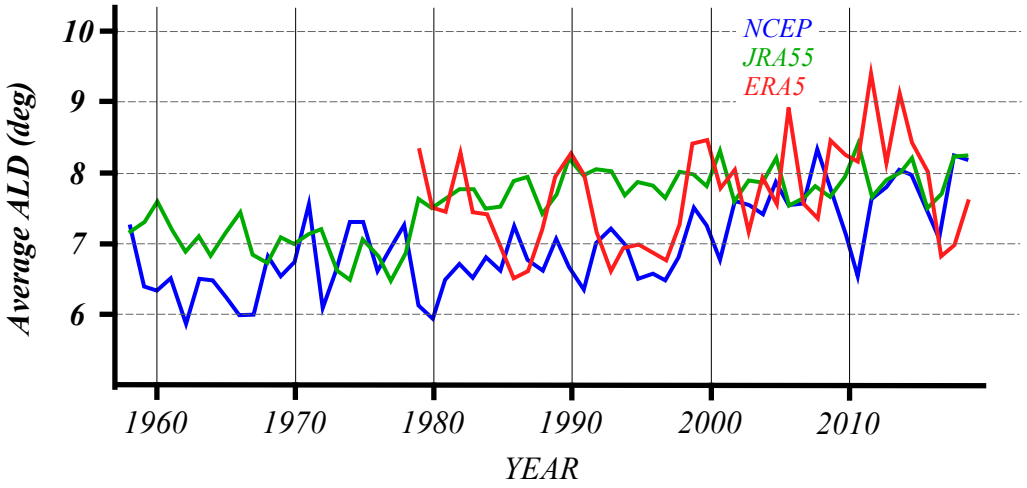

Figure 14: Seasonal average ALD (in degrees) of the Southern Hemisphere unimodal warm season jet (November – April) for each of the different reanalyses..

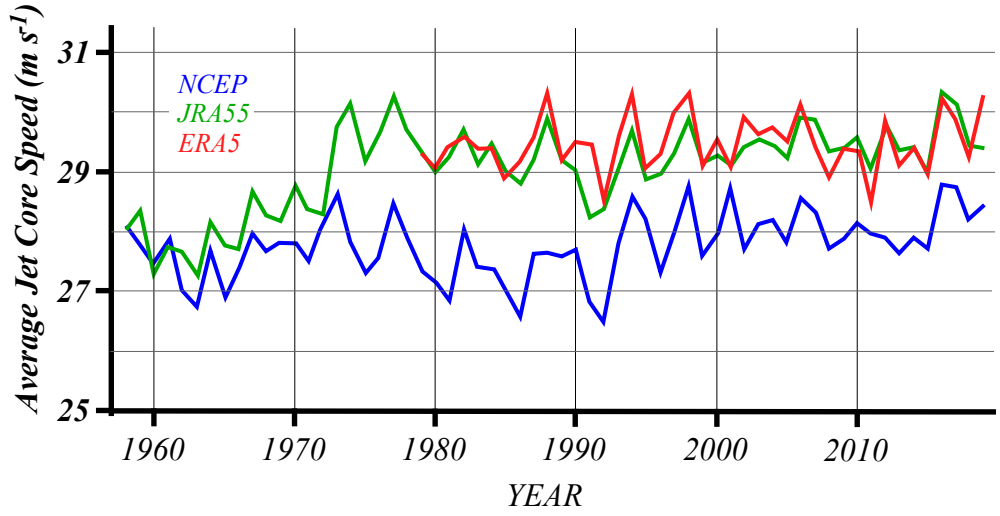

Figure 15: Seasonal average wind speed (m s^{-1}) along the core isertel of the Southern Hemisphere warm season (November – April) unimodal jet for each of the different reanalyses.

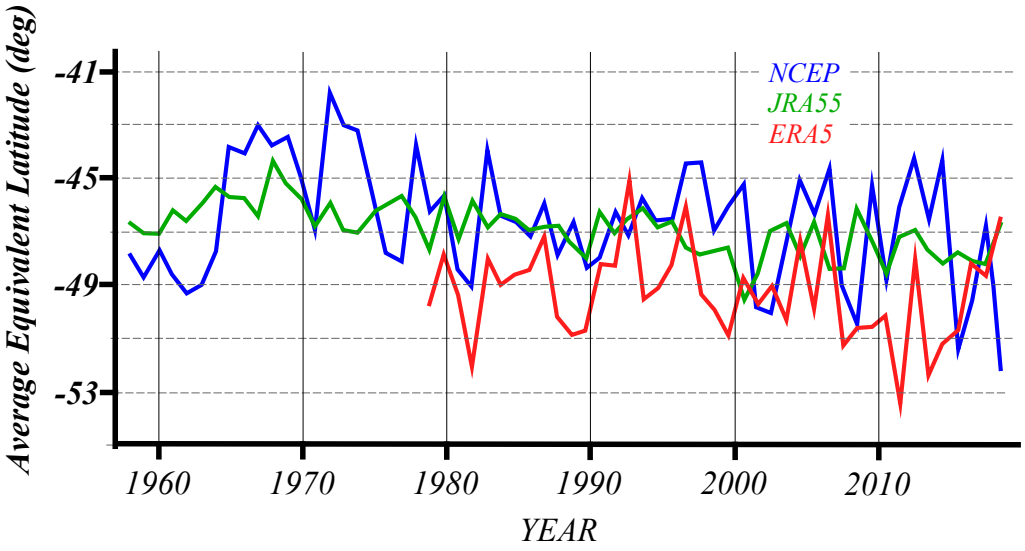

Figure 16: Seasonal average equivalent latitude of the Southern Hemisphere unimodal warm season (November – April) jet for each of the different reanalyses.

The interannual variability in the seasonal average equivalent latitude is a bit more of a conundrum. It is tempting to dismiss the pre-satellite era calculations as unreliable as a result of basic observational constraints. However, even in the satellite era much larger interannual variability characterizes this measure for the SH warm season jet than for its NH counterpart. In the absence of other compelling first order explanations, this difference may be a signal of a more fundamental contrast in the warm season circulations characteristic of both hemispheres. Indeed, some support for this view arises from the fact that Naud et al. (2023) found substantially more occluded cyclones in SH summer than in NH summer.

4. Conclusions and Discussion

The analysis presented here primarily focuses on elucidating the nature of the NH, warm season (MJJASO), tropopause-level jet stream and assessing trends in a number of its characteristics as represented by three reanalysis data sets. Following the methodology of Christenson et al. (2017), the present analysis creates a warm season tropopause-level jet identification in θ/PV space for the first time. A prominent result of this analysis is that in all three of the reanalysis data sets assessed, a single peak in the frequency of occurrence of qualifying column-maximum wind speeds partitioned among 5K isentropic layers suggests that the warm season in both hemispheres is characterized by a single tropopause-level jet stream (Figs. 1,5, and 6) as opposed to the well-documented bimodal distribution composed of separate polar and subtropical jets that characterize their cold seasons (i.e., Strong and Davis 2007, Christenson et al. 2017, Martin 2021, Martin and Norton 2023

and several references therein). The single, or unimodal, NH warm season jet generally resides in the 330–345 K isentropic layer, a slightly lower layer than that containing the cold season subtropical jet, and is a characteristic evident in all three data sets. It does, however, exhibit some minor variations in the first and last months of the warm season, first residing in the slightly lower 325–340 K layer in May, returning to 330–345 K for the next few months, and moving back to the 325–340 K layer in October. Over a full calendar year in the NH, only five (out of 54) isentropic layers differ across the three data sets (as seen in Table 1). Similarity amongst the data sets extends to their respective characterizations of the April/November transitions between the bimodal and unimodal NH jets as well (Figs. 2 and 3).

With the isentropic housing of the warm season unimodal jet in hand, the ALD method of Martin (2021) was employed to explore a number of characteristics of the NH warm season jet, to the best of the authors' knowledge, for the first time. The waviness of the jet was found to have decreased slightly in the pre-satellite era with both data sets exhibiting significance to at least the 90% level. In the satellite era, however, waviness increased in all three data sets though the trend was only significant in the ERA5 and NCEP reanalyses. Consequently, we concluded that there has been a very slight increase in the waviness of the warm season unimodal jet over the last 4 decades.

Trends in the seasonal average jet core wind speed, the speed of the flow along each day's core isertel, were not uniform across the three data sets. Both pre-satellite era time series showed modest, statistically significant increases in the jet speed. However, in the satellite era the signal is rather mixed. The NCEP trend is almost flat and statistically insignificant whereas more substantial, but still modest, decreases were present in the JRA-55 and ERA5 data, with only ERA5 trends exhibiting significance. Thus, the analysis concludes that the warm season unimodal jet has undergone a very slight decrease in speed over the last 40 years. Coupled with the slightly increased waviness, this suggests that a nearly steady circulation has stirred the NH warm season midlatitudes over the last 40 years.

Finally, evidence of latitudinal migration of the NH warm season jet can be garnered from consideration of the time series of equivalent latitude. Once again, the pre-satellite and satellite eras exhibit different tendencies. In the former, though there is some disparity between the individual NCEP and JRA-55 time series, both exhibit a similar decrease (i.e. equatorward migration) that is statistically significant. However, in the satellite era, only the NCEP and JRA-55 data sets feature a similar slightly increasing trend whereas ERA5 exhibits a slight decrease. *None* of those trends are significant. Thus, it appears that the NH warm season unimodal jet has been relatively stationary — residing near ~41°N over the past four decades.

Unsurprisingly, of the three reanalysis data sets employed here the NCEP reanalysis frequently stands apart from the other two. It has a narrower distribution of daily core isertels (Fig. 9), higher seasonal average waviness (Fig. 10), and a more poleward equivalent latitude (Fig. 12) than the other two reanalyses. Fundamental differences in both the spatial resolution of and the degraded representation of physical processes at its lower resolution in the NCEP data compared to the other two likely underlie some of the discrepancies revealed in the analysis.

Martin (2021) applied the ALD methodology to analysis of the NH cold season (DJF) jets using the same three data sets. He found that no significant trends in average speed were present in any of the three data sets for either the polar or

subtropical jets in the cold season. However, both jets were found to be experiencing a systematic increase in waviness over time. Thus, trends in the behavior of the warm season unimodal jet are quite distinct from those of the two cold season jets suggesting that seasonality may modulate any broad tendencies that might otherwise be induced by a slow background climate change.

Other recent studies have offered evaluation of trends in various warm season jet characteristics employing other methods of jet identification and assessment (e.g., Strong and Davis 2007; Archer and Caldeira 2008; Manney and Hegglin 2018; Martin 2021). While not emphasizing a distinction between a subtropical and polar jet in their analysis of the NH jet, Archer and Caldeira (2008) showed a subtle poleward encroachment and slight decrease in speed for the summertime (JJA) jet in their analysis – similar to what was found here. The analysis of Manney and Hegglin (2018) incorporates a latitudinal criteria on jet identification that, quite unlike the present identification method, guarantees the existence of a polar jet during the warm season. They found that in the Northern Hemisphere summer (JJA) the polar jet speed decreases over North America and the Atlantic while moving equatorward – in opposition to the results of the present analysis. The fact that the jet identification methodology in the present study has little overlap with that employed by Manney and Hegglin (2018) likely underlies at least some of the resulting differences in the respective analyses.

Though a basic picture of the warm season unimodal jet emerges from the analyses presented here, a number of fundamental issues remain to be examined. Perhaps chief among them is a more detailed understanding of the transition from bimodal to unimodal, and vice versa, that characterizes the NH jet in April and November, respectively. The residence of the warm season unimodal jet in the 330–345K layer, a layer that lies between the separate cold season polar and subtropical jets, invites the suggestion that it is a hybrid of those formerly separate jets or that one or the other of the cold season features disappears in the warm season. The fact that tropical temperatures and humidities routinely encroach on high latitudes during summer implies that the unimodal warm season jet is a slightly transformed subtropical jet. Better understanding of the nature of these annual transitions, as well as the characteristic sensible weather consequences that accompany them, is an important topic for subsequent work. Additionally, as the climate continues to warm it may be that the annual presence of the unimodal jet will expand changing the timing and perhaps the nature of the transition periods and their associated sensible weather. Investigation of both of these issues, employing the output from the Community Earth System Model Large Ensemble (CESM-LE), is currently underway.

The same climate model output is also being employed in the analysis of future changes in the waviness, jet core speed, and average latitude of the warm season unimodal jet. By virtue of the jet's relationship to the development, severity, and distribution of a variety of organized convective disturbances, its evolving characteristics are likely to exert a substantial impact on future warm season sensible weather in the middle latitudes. Additionally, though the ALD method was developed to conduct a hemispheric analysis of jet characteristics, it can be applied regionally as well. Thus, direct comparison of regional trends derived from this method can be made, for instance, to the regional results of Manney and Hegglin (2018).

Code and data availability

For the present analysis the code was restructured and formatted to Python by the first author. The software was originally developed in GEMPAK by the second author. Both forms of software written to perform the analysis are available from the authors upon request. ERA5 data are available from the Copernicus Climate Change Service Climate Data Store (CDS) at https://cds. climate.copernicus.eu/cdsapp#!/home (Copernicus Climate Change Service (C3S), 2017). JRA-55 data are provided by the Research Data Archive at the National Center for Atmospheric Research (https://doi.org/10.5065/D6HH6H41, NCAR, 2013). NCEP/NCAR Reanalysis data were made available by the NOAA/OAR/ESRL PSL Boulder, CO, and are available at https://psl.noaa.gov/data/gridded/data.ncep.reanalysis.html (NOAA, 2020).

Author contributions

LJO performed the analysis, drafted the article, created several figures, and prepared the manuscript for submission. JEM devised the original methodology, contributed to revising the article, and created the time series figures.

Competing interests

The authors declare that they have no conflict of interest.

Disclaimer

"Copernicus Publications remains neutral with regard to jurisdictional claims made in the text, published maps, institutional affiliations, or any other geographical representation in this paper. While Copernicus Publications makes every effort to include appropriate place names, the final responsibility lies with the authors. Views expressed in the text are those of the authors and do not necessarily reflect the views of the publisher."

Acknowledgements

This work was supported by the National Science Foundation under grant no. 2055667

Financial support

This research has been supported by the National Science Foundation (grant no. 2055667)

Plain Language Summary

Two separate jet structures, the polar and subtropical jets, characterize the cold season of both hemispheres. This study reveals that the dual-jet structure doesn't persist through the hemispheres' warm seasons. Instead, with the apparent erosion of the polar jet, the warm seasons are characterized by a single tropopause-level jet. Trends in waviness, average speed, and latitudinal location of this unimodal warm season jet are examined in time series analyses of three reanalysis data sets.

References

Alpert, P., and E. Ganor, 1993: A jet stream associated heavy dust storm in the western Mediterranean. Journal of Geophysical Research: Atmospheres, 98, 7339–7349, https://doi.org/10.1029/92JD01642.

Archer, C. L., and K. Caldeira, 2008: Historical trends in the jet streams. Geophysical Research Letters, 35, https://doi.org/10.1029/2008GL033614.

Athanasiadis, P. J., J. M. Wallace, and J. J. Wettstein, 2010: Patterns of Wintertime Jet Stream Variability and Their Relation to the Storm Tracks. https://doi.org/10.1175/2009JAS3270.1.

Barnes, E. A., 2013: Revisiting the evidence linking Arctic amplification to extreme weather in midlatitudes. Geophysical Research Letters, 40, 4734–4739, https://doi.org/10.1002/grl.50880.

——, and L. Polvani, 2013: Response of the Midlatitude Jets, and of Their Variability, to Increased Greenhouse Gases in the CMIP5 Models. https://doi.org/10.1175/JCLI-D-12-00536.1.

Barnes, E. A., and J. A. Screen, 2015: The impact of Arctic warming on the midlatitude jet-stream: Can it? Has it? Will it? WIREs Climate Change, 6, 277–286, https://doi.org/10.1002/wcc.337.

Blackport, R., and J. A. Screen, 2020: Insignificant effect of Arctic amplification on the amplitude of midlatitude atmospheric waves. https://doi.org/10.1126/sciadv.aay2880.

Burt, M. A., D. A. Randall, and M. D. Branson, 2016: Dark Warming. J. Climate, 29, 705–719, https://doi.org/10.1175/JCLI-D-15-0147.1.

Christenson, C. E., J. E. Martin, and Z. J. Handlos, 2017: A Synoptic Climatology of Northern Hemisphere, Cold Season Polar and Subtropical Jet Superposition Events. https://doi.org/10.1175/JCLI-D-16-0565.1.

Clark, A. J., C. J. Schaffer, W. A. Gallus, and K. Johnson-O'Mara, 2009: Climatology of Storm Reports Relative to Upper-Level Jet Streaks, https://doi.org/10.1175/2009WAF2222216.1.

Copernicus Climate Change Service (C3S). (2017). ERA5: Fifth generation of ECMWF atmospheric reanalyses of the global climate. Copernicus Climate Change Service Climate Data Store (CDS). Retrieved from https://cds.climate.copernicus.eu/cdsapp#!/home

Coumou, D., V. Petoukhov, S. Rahmstorf, S. Petri, and H. J. Schellnhuber, 2014: Quasi-resonant circulation regimes and hemispheric synchronization of extreme weather in boreal summer. Proceedings of the National Academy of Sciences, 111, 12331–12336, https://doi.org/10.1073/pnas.1412797111.

Cunningham, P., and D. Keyser, 2004: Dynamics of jet streaks in a stratified quasi-geostrophic atmosphere: Steady-state representations. Quarterly Journal of the Royal Meteorological Society, 130, 1579–1609, https://doi.org/10.1256/qj.03.35.

Davies, H. C., and A. M. Rossa, 1998: PV Frontogenesis and Upper-Tropospheric Fronts. Monthly Weather Review, 126, 1528–1539. https://doi.org/10.1175/1520-0493(1998)126<1528:pfautf>2.0.co;2

Defant, F., and H. Taba, 1957: The Threefold Structure of the Atmosphere and the Characteristics of the Tropopause. *Tellus*, 9, https://doi.org/10.3402/tellusa.v9i3.9112.

Ertel, H. (1942). Ein Neuer hydrodynamischer Wirbelsatz. Meteorologische Zeitschrift, 59, 271–281.

Francis, J. A., 2017: Why Are Arctic Linkages to Extreme Weather Still up in the Air? https://doi.org/10.1175/BAMS-D-17-0006.1.

Francis, J. A., N. Skific, and S. J. Vavrus, 2018: North American Weather Regimes Are Becoming More Persistent: Is Arctic Amplification a Factor? Geophysical Research Letters, 45, 11,414-11,422, https://doi.org/10.1029/2018GL080252.

Handlos, Z. J., and J. E. Martin, 2021: Composite Life Cycle of West Pacific Jet-Superposition Events and the Large-Scale Environmental Response over Western North America, https://doi.org/10.1175/MWR-D-20-0130.1.

Harnik, N., Garfinkel, C. I., Lachmy, O., 2016: The influence of jet stream regime on extreme weather events. Dynamics and Predictability of Large-Scale, High-Impact, Weather and Climate Events, Li, J., Swinbank, R., Grotjahn, R., Volkert, H., Cambridge University Press, 79-94.

Held, I. M., 1975: Momentum Transport by Quasi-Geostrophic Eddies. Journal of the Atmospheric Sciences, 32, 1494–1497. https://doi.org/10.1175/1520-0469(1975)032<1494:mtbqge>2.0.co;2

——, and A. Y. Hou, 1980: Nonlinear Axially Symmetric Circulations in a Nearly Inviscid Atmosphere. Journal of the Atmospheric Sciences, 37, 515–533. https://doi.org/10.1175/1520-0469(1980)037<0515:nascia>2.0.co;2

Homeyer, C. R., K. P. Bowman, and L. L. Pan, 2010: Extratropical tropopause transition layer characteristics from high-resolution sounding data. Journal of Geophysical Research: Atmospheres, 115, https://doi.org/10.1029/2009JD013664.

Hoskins, B., and P. Berrisford, 1988: A Potential Vorticity Perspective of the Storm of 15–16 October 1987. Weather, 43, 122–129, https://doi.org/10.1002/j.1477-8696.1988.tb03890.x.

Hoskins, B. J., M. E. McIntyre, and A. W. Robertson, 1985: On the use and significance of isentropic potential vorticity maps. Quarterly Journal of the Royal Meteorological Society, 111, 877–946, https://doi.org/10.1002/qj.49711147002.

Kalnay, E., and Coauthors, 1996: The NCEP/NCAR 40-Year Reanalysis Project. Bulletin of the American Meteorological Society, 77, 437–471. https://doi.org/10.1175/1520-0477(1996)077<0437:tnyrp>2.0.co;2

Keyser, D., and M. A. Shapiro, 1986: A review of the structure and dynamics of upper-level frontal zones. Mon. Wea. Rev., 114, 452–499, https://doi.org/10.1175/1520-0493(1986)114<0452:AROTSA>2.0.CO;2

Krishnamurti, T. N., and H. N. Bhalme, 1976: Oscillations of a Monsoon System. Part I. Observational Aspects. J. Atmos. Sci., 33, 1937–1954, https://doi.org/10.1175/1520-0469(1976)033<1937:OOAMSP>2.0.CO;2.

Kistler, R., and Coauthors, 2001: The NCEP–NCAR 50-Year Reanalysis: Monthly Means CD-ROM and Documentation. Bulletin of the American Meteorological Society, 82, 247–267. https://doi.org/10.1175/1520-0477(2001)082<0247:tnnyrm>2.3.co;2

Kobayashi, S., and Coauthors, 2015: The JRA-55 Reanalysis: General Specifications and Basic Characteristics. Journal of the Meteorological Society of Japan, 93, 5–48, https://doi.org/10.2151/jmsj.2015-001.

Koch, P., H. Wernli, and H. Davies, 2006: An Event-based jet-stream climatology and typology. International Journal of Climatology, 26, 283–301, https://doi.org/10.1002/joc.1255.

Manney, G. L., and M. I. Hegglin, 2018: Seasonal and Regional Variations of Long-Term Changes in Upper-Tropospheric Jets from Reanalyses. https://doi.org/10.1175/JCLI-D-17-0303.1.

Manney, G. L., and Coauthors, 2011: Jet characterization in the upper troposphere/lower stratosphere (UTLS): applications to climatology and transport studies. Atmospheric Chemistry and Physics, 11, 6115–6137, https://doi.org/10.5194/acp-11-6115-2011.

Manney, G. L., M. I. Hegglin, W. H. Daffer, M. J. Schwartz, M. L. Santee, and S. Pawson, 2014: Climatology of Upper Tropospheric–Lower Stratospheric (UTLS) Jets and Tropopauses in MERRA. https://doi.org/10.1175/JCLI-D-13-00243.1.

——, and Coauthors, 2017: Reanalysis comparisons of upper tropospheric–lower stratospheric jets and multiple tropopauses. Atmospheric Chemistry and Physics, 17, 11541–11566, https://doi.org/10.5194/acp-17-11541-2017.

Martin, J. E., 2021: Recent Trends in the Waviness of the Northern Hemisphere Wintertime Polar and Subtropical Jets. Journal of Geophysical Research: Atmospheres, 126, e2020JD033668, https://doi.org/10.1029/2020JD033668.

Martin, J. E., and T. Norton, 2023: Waviness of the Southern Hemisphere wintertime polar and subtropical jets. Weather and Climate Dynamics, 4, 875–886, https://doi.org/10.5194/wcd-4-875-2023.

McWilliams, J. C., and J. H. S. Chow, 1981: Equilibrium Geostrophic Turbulence I: A Reference Solution in a β-Plane Channel. J. Phys. Oceanogr., 11, 921–949, https://doi.org/10.1175/1520-0485(1981)011<0921:EGTIAR>2.0.CO;2

Miller, R. L., G. A. Schmidt, and D. T. Shindell, 2006: Forced annular variations in the 20th century Intergovernmental Panel on Climate Change Fourth Assessment Report models. Journal of Geophysical Research: Atmospheres, 111, https://doi.org/10.1029/2005JD006323.

Morgan, M. C., and J. W. Nielsen-Gammon, 1998: Using Tropopause Maps to Diagnose Midlatitude Weather Systems. Mon. Wea. Rev., 126, 2555–2579, https://doi.org/10.1175/1520-0493(1998)126<2555:UTMTDM>2.0.CO;2

Nakamura, H., and A. Shimpo, 2004: Seasonal Variations in the Southern Hemisphere Storm Tracks and Jet Streams as Revealed in a Reanalysis Dataset. Journal of Climate, 17, 1828-1844, https://doi.org/10.1175/1520-0442(2004)017<1828:SVITSH>2.0.CO;2

Naidu, C. V., K. M. Krishna, S. R. Rao, O. S. R. U. Bhanu Kumar, K. Durgalakshmi, and S. S. V. S. Ramakrishna, 2011: Variations of Indian summer monsoon rainfall induce the weakening of easterly jet stream in the warming environment? Global and Planetary Change, 75, 21–30, https://doi.org/10.1016/j.gloplacha.2010.10.001.

Namias, J., and P. F. Clapp, 1949: Confluence theory of the high tropospheric jet stream. J. Meteor., 6, 330–336, https://doi.org/10.1175/1520-0469(1949)006<0330:CTOTHT>2.0.CO;2

Naud, C. M., J. E. Martin, P. Ghosh, G. Elsaesser, and D. Posselt, 2023: Automated identification of occluded sectors in midlatitude cyclones: Method and some climatological applications. Quarterly Journal of the Royal Meteorological Society, 149, 1990–2010, https://doi.org/10.1002/qj.4491.

NCAR: JRA-55: Japanese 55-year Reanalysis, Daily 3-Hourly and 6-Hourly Data, NCAR [data set], https://doi.org/10.5065/D6HH6H41, 2013.

Newton, C. W., 1954: Frontogenesis and frontolysis as a three-dimensional process. J. Meteor., 11, 449–461, https://doi.org/10.1175/1520-0469(1954)011<0449:FAFAAT>2.0.CO;2.

NOAA: NCEP-NCAR Reanalysis, NOAA [data set], https:// psl.noaa.gov/data/gridded/data.ncep.reanalysis.html, last access: October 2020.

Palmén, E.H. and Newton, C.W. (1969) Atmospheric Circulation Sys-tems: Their Structure and Physical Interpretation, Vol. 13. Academic press.

Panetta, R. L. (1993). Zonal jets in wide baroclinically unstable regions: Persistence and scale selection. Journal of the Atmospheric Sciences, 50, 2073–2106. https://doi.org/10.1175/1520-0469(1993)050<2073:zjiwbu>2.0.co;2

Petoukhov, V., S. Rahmstorf, S. Petri, and H. J. Schellnhuber, 2013: Quasiresonant amplification of planetary waves and recent Northern Hemisphere weather extremes. Proceedings of the National Academy of Sciences, 110, 5336–5341, https://doi.org/10.1073/pnas.1222000110.

Randel, W. J., D. J. Seidel, and L. L. Pan, 2007: Observational characteristics of double tropopauses. Journal of Geophysical Research: Atmospheres, 112, https://doi.org/10.1029/2006JD007904.

Rhines, P. B., 1975: Waves and turbulence on a beta-plane. Journal of Fluid Mechanics, 69, 417–443, https://doi.org/10.1017/S0022112075001504.

Roja Raman, M., V. V. M. Jagannadha Rao, M. Venkat Ratnam, M. Rajeevan, S. V. B. Rao, D. Narayana Rao, and N. Prabhakara Rao (2009), Characteristics of the Tropical Easterly Jet: Long-term trends and their features during active and break monsoon phases, J. Geophys. Res., 114, D19105, doi:10.1029/2009JD012065.

Röthlisberger, M., S. Pfahl, and O. Martius, 2016: Regional-scale jet waviness modulates the occurrence of midlatitude weather extremes. Geophysical Research Letters, 43, 10,989-10,997, https://doi.org/10.1002/2016GL070944.

Santer, B. D., J. J. Hnilo, T. M. L. Wigley, J. S. Boyle, C. Doutriaux, M. Fiorino, D. E. Parker, and K. E. Taylor, 1999: Uncertainties in observationally based estimates of temperature change in the free atmosphere. Journal of Geophysical Research: Atmospheres, 104, 6305–6333, https://doi.org/10.1029/1998JD200096.

Screen, J. A., and I. Simmonds, 2010: The central role of diminishing sea ice in recent Arctic temperature amplification. Nature, 464, 1334–1337, https://doi.org/10.1038/nature09051.

——, and ——, 2013: Exploring links between Arctic amplification and mid-latitude weather. Geophysical Research Letters, 40, 959–964, https://doi.org/10.1002/grl.50174.

——, and ——, 2014: Amplified mid-latitude planetary waves favour particular regional weather extremes. Nature Clim Change, 4, 704–709, https://doi.org/10.1038/nclimate2271.

Serreze, M. C., A. P. Barrett, J. C. Stroeve, D. N. Kindig, and M. M. Holland, 2009: The emergence of surface-based Arctic amplification. The Cryosphere, 3, 11–19, https://doi.org/10.5194/tc-3-11-2009.

Shapiro, M. A., and Coauthors, 1999: A planetary-scale to mesoscale perspective of the life cycles of extratropical cyclones: The bridge between theory and observations. The Life Cycle of Extratropical Cyclones, M. A. Shapiro and S. Gronas, Eds., Amer. Meteor. Soc., 139–185.

Shapiro, M. A., and D. Keyser, 1990: Fronts, jet streams and the tropopause. Extratropical Cyclones: The Erik Palmen Memorial Volume, C. Newton and E. O. Holopainen, Eds., Amer. Meteor. Soc., 167–191.

Strong, C., and R. E. Davis, 2007: Winter jet stream trends over the Northern Hemisphere. Quarterly Journal of the Royal Meteorological Society, 133, 2109–2115, https://doi.org/10.1002/qj.171.

Sturaro, G., 2003: A closer look at the climatological discontinuities present in the NCEP/NCAR reanalysis temperature due to the introduction of satellite data. Climate Dynamics, 21, 309–316, https://doi.org/10.1007/s00382-003-0334-4.

Swart, N. C., and J. C. Fyfe, 2012: Observed and simulated changes in the Southern Hemisphere surface westerly wind-stress. Geophysical Research Letters, 39, https://doi.org/10.1029/2012GL052810.

Vavrus, S. J., 2018: The Influence of Arctic Amplification on Mid-latitude Weather and Climate. Curr Clim Change Rep, 4, 238–249, https://doi.org/10.1007/s40641-018-0105-2.

Whitney, L. F., 1977: Relationship of the Subtropical Jet Stream to Severe Local Storms. Mon. Wea. Rev., 105, 398-412, https://doi.org/10.1175/1520- 0493(1977)105<0398:ROTSJS>2.0.CO;2

Winters, A. C., D. Keyser, L. F. Bosart, and J. E. Martin, 2020: Composite Synoptic-Scale Environments Conducive to North American Polar–Subtropical Jet Superposition Events, https://doi.org/10.1175/MWR-D-19-0353.1.

Woollings, T., and M. Blackburn, 2012: The North Atlantic Jet Stream under Climate Change and Its Relation to the NAO and EA Patterns. https://doi.org/10.1175/JCLI-D-11-00087.1.

Yin, J. H., 2005: A consistent poleward shift of the storm tracks in simulations of 21st century climate. Geophysical Research Letters, 32, https://doi.org/10.1029/2005GL023684.